ANL/CFCT-20/16

# Mechanistic Source Term Development for Liquid Fueled MSRs - Model Development Update

Chemical and Fuel Cycle Technologies Division

ANL/CFCT-20/16

# Mechanistic Source Term Development for Liquid Fueled MSRs - Model Development Update

Prepared by
Sara Thomas, James Jerden
Chemical and Fuel Cycle Technologies Division, Argonne National Laboratory

July 15, 2020

# Table of Contents

# 1 Introduction: Objectives and Approach

## *1.1 Background*

This report provides results from a critical literature review on the development of a mechanistic source term model (MST) for liquid fueled molten salt reactors (MSRs). It is submitted in fulfillment of milestone M4AT-20AN040601075 in the Advanced Reactor Technologies Molten Salt Reactors Campaign work package AT-20AN04060107.

Source term estimation is essential for reactor licensing [NRC, 1995] and is defined in 10 CFR § 50.2 as:

> *"The magnitude and mix of the radionuclides released from the fuel, expressed as fractions of the fission product inventory in the fuel, as well as their physical and chemical form, and the timing of their release."*

Source term analyses are used to evaluate the consequences of licensing basis events involving normal reactor operations, anticipated off-normal conditions, design basis transients, and beyond design basis transient scenarios. In addition, source term analyses can play a key role in reactor siting and the development of emergency planning zones and reactor site boundaries [NRC 1993, NRC 2003, NRC 2005]. For new generation advanced reactor concepts, source term analyses can provide valuable feedback into the design process and facilitate risk-informed engineering decisions (e.g., Yoshioka et al., 2012, Grabaskas et al., 2016a, Gérardin et al., 2019).

Traditionally, source term analyses for light water reactors (LWRs) have used conservative bounding assumptions (e.g., NRC, 1995). However, for a source term analysis to provide useful feedback into the reactor design process and justify minimizing the size of reactor site emergency planning zones, it must involve more realistic (i.e., mechanistic) models that do not require conservative assumptions regarding radionuclide release during postulated accidents and transients.

The NRC has recognized the need for mechanistic source term (MST) analyses since the 1990s (e.g., NRC, 1993; NRC, 2003; NRC, 2005). Although no formal definition for MST has been established, the NRC has described an MST in SECY-93-092 (NRC, 1993) as:

> *"…the result of an analysis of fission product release based on the amount of cladding damage, fuel damage, and core damage resulting from the specific accident sequences being evaluated. It is developed using best-estimate phenomenological models of the transport of the fission products from the fuel through the reactor coolant system, through all holdup volumes and barriers, taking into account mitigation features, and finally, into the environs."*

Such models are referred to as mechanistic because they take into account the real transport/retention processes (e.g., solubility, precipitation, vaporization, adsorption, aerosolization) based on fundamental chemistry (e.g., thermodynamics, electrochemistry, kinetics).

NRC staff recommendations for new license applications for advanced reactors established the essential characteristics of an MST (NRC, 1993):

> *"…source terms should be based upon a mechanistic analysis and will be based on the staff's assurance that the provisions of the following three items are met:*

- *The performance of the reactor and fuel under normal and off-normal conditions is sufficiently well understood to permit a mechanistic analysis. Sufficient data should exist on the reactor and fuel performance through the research, development, and testing programs to provide adequate confidence in the mechanistic approach.*
- *The transport of fission products can be adequately modeled for all barriers and pathways to the environs, including specific consideration of containment design. The calculations should be as realistic as possible so that the values and limitations of any mechanisms or barrier are not obscured.*
- *The events considered in the analyses to develop the set of source terms for each design are selected to bound severe accidents and design-dependent uncertainties."*

The history of source term model development from a regulatory perspective is discussed in Section 2.

### *1.2 Objectives and Approach*

The primary challenge to developing MSTs for non-LWR advanced reactor concepts is that it likely requires the development of new modeling tools (or the significant alteration of existing codes) and may require a significant experimental program to obtain the fundamental chemical and transport data needed to implement mechanistic models. Initial work defining data needs for the development of an MST model for liquid fueled MSRs was discussed in Jerden et al., 2019a and an experimental program providing the type of thermophysical, thermochemical, and modeling tools has been implemented within the Molten Salt Reactors Campaign. This report provides an in-depth critical review of the information sources that will form the basis for a state-of-the-art MST model for liquid fueled MSRs.

This is done by reviewing technical information that will be used to develop a technology inclusive methodology for evaluating MSTs for sets of bounding accident scenarios for liquid fueled MSRs. The methodology developed will be applicable to both fluoride and chloride fueled reactors. The bounding accidents of interest have been identified and discussed in Shahbazi and Grabaskas, 2020 and are summarized as follows:

- *Rupture of the fuel salt loop*: A break in the reactor core vessel would cause fission product and actinide-bearing salt to flow onto the floor of the core containment cell. Most MSR designs will have a guard vessel or core catcher to avoid the undesirable interaction of the fuel salt with concrete. Directly pouring large amounts of fuel salt onto concrete would result in concrete dehydration and gas generation that would increase containment pressurization. MSRs can include gravity fed subcritical drain tank(s) to capture the released fuel salt and the core catcher can be sloped to direct spilled fuel salt to flow into the drain tanks. The fuel salt decay heat must be removed whether the salt remains in the fuel salt loop or has been spilled into the guard vessel, core catcher, or drain tank. The rate of decay heat removal and the fate of semi-volatile radionuclides are key unknowns that need to be quantified and experimentally validated.

- *Rupture of the primary heat exchanger tubing*: In many MSR designs, the fuel salt is only separated from the coolant by thin-walled heat exchanger tubing. Failure of the primary heat exchanger tubing could provide a path for fuel salt radionuclides to bypass outer containment layers and allow coolant fluid (which may or may not be a salt) to mix with the fuel salt. The coolant would be kept at a higher pressure than the fuel salt to ensure that flow is inward and maintain the radionuclide retention fundamental safety function. A second break in the fuel salt loop would be required for most of the coolant to leak into containment layers because inflow would stop once the fuel salt loop has filled to capacity.

- *Rupture in cover gas/off gas system*: MSRs generally have two cover gas system design variants relevant to bounding accident progression. In the first, the fission gases are removed from the reactor vessel only after a period of decay. The purpose for the eventual removal is to avoid pressurization of the fuel salt circuit. The principal alternative design is to rapidly remove gases emerging from the fuel salt from the reactor vessel. This design slows the build-up of fission products in the salt and reduces the quantity of labile radionuclides within the vessel. While removing radionuclides from the vessel does decrease the amount that can be released in the event of a core related accident, the radionuclides will increase its decay heat removal requirements for the cover gas handling system and increase the consequences from a cover gas system leak.

- *Rupture in fuel processing system*: Accidents in the fuel processing system could compromise radionuclide containment in the interconnected MSR fuel salt loop by introducing corrosive materials or unanticipated amounts of fissile materials in the returned fuel salt. The corrosive materials that were planned for use in the molten salt breeder reactor (MSBR) fuel processing system included fluorine gas, hydrogen fluoride, and liquid bismuth. Introducing any of these into the fuel salt loop would rapidly corrode the container alloy. Excessive amounts of fissile material could be returned to the fuel salt loop by rapidly introducing fissile materials that have been stored (either intentionally or inadvertently) in the fuel processing system. This would cause a reactivity excursion.

Developing an MST model that includes possible radionuclide dispersal during the bounding accidents described above will involve the integration of best-estimate phenomenological models of radionuclide transport from the fuel to the environment that take holdup volumes, barriers to release, and phenomena that inhibit or slow transport into account.

By providing a state-of-the-art assessment of the current knowledge base and computational tools needed to quantify the complex physical and chemical phenomena needed to implement an MST for MSRs (including aerosol and mist formation and transport), the current project to develop MST models will clarify issues identified in the NRC review of DG-1353 and NEI 18-04.

The development of a generic MST modeling capability for MSRs will involve the following steps:

1. Identify and characterize radionuclide sources, partitioning phenomena and possible release pathways for bounding accident scenarios discussed in Sections 3 and 4.
2. Identify functional needs for a generic technology-inclusive MST for MSRs.
3. Identify and characterize knowledge gaps and gaps in existing codes that need to be filled to implement a robust technology-inclusive MST model.
4. Recommend experimental and code development programs for filling knowledge/code gaps.

The MST approach to source term calculations allows vendors to realistically assess radiological consequences of accident scenarios. The model results may thereby inform design decisions that mitigate possible radionuclide release phenomena and could ultimately provide justifications for smaller exclusion areas and low population zones when siting the reactor (SECY-16-0012).

As mentioned above, the development of the MSR MST assessment capability discussed in this report builds on the successful MST evaluation of the sodium fast reactor (SFR) concept developed as part of the DOE Advanced Reactor Technology, Regulatory Technology Development Plan (Grabaskas et al., 2015, Grabaskas et al., 2016a and Grabaskas et al., 2016b). The general methodology for MSR MST is summarized in Figure 1.

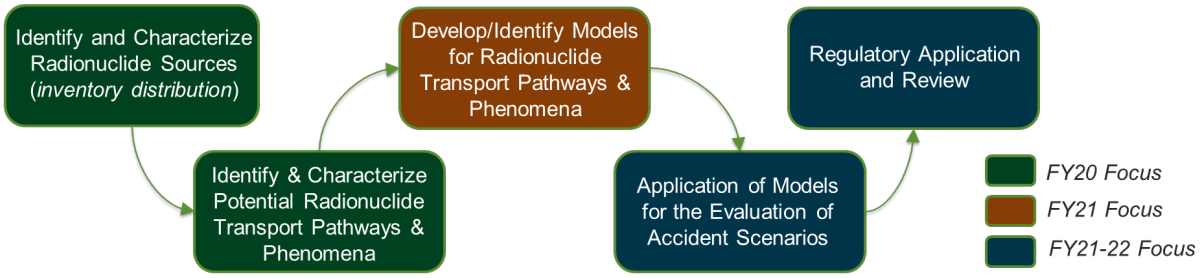


**Figure 1**. Methodology for developing a mechanistic source term assessment capability for MSRs.

Meeting the objectives listed above and identified in Figure 1 involves on-going critical reviews of the historical MSR literature, a review of publicly available information on the newer MSR concepts, and input from experimental and modeling efforts being performed as part of the DOE MSR campaign.

The inputs and links between the ongoing DOE Advanced Reactor Technologies, Molten Salt Reactors Campaign experimental and modeling projects and MST development efforts described in this report are summarized in Figure 2.

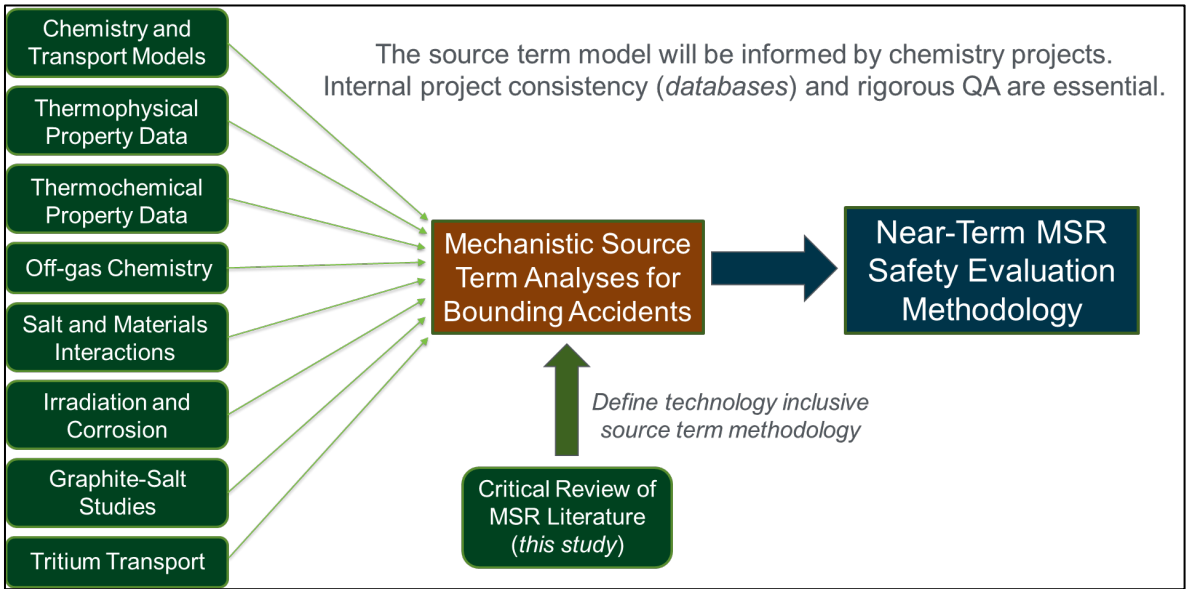


Figure 2. Schematic diagram showing inputs from salt chemistry studies needed to develop and parameterize an MST model for MSRs.

## 2 Historical Survey of the Use of Mechanistic Source Term Assessments for NPPs

The following section provides a historical survey and summary of the development of the concept of MST and regulatory context for the subsequent technical discussions. MST is essential in the modern licensing process for nuclear power plants (NPPs) and has been a focus of previous licensing efforts. Source term was first developed in the early stages of the U.S. commercial industry in the 1960s using conservative assumptions and data available at the time. As technology advanced and the state of knowledge improved, adjustments to source term were necessary and stressed a more realistic, mechanistic approach. The history

of the regulations that pertain to source term for use in NPP licensing is discussed in this section with a particular focus on MST. A description of relevant NRC documents is presented in Figure 3.

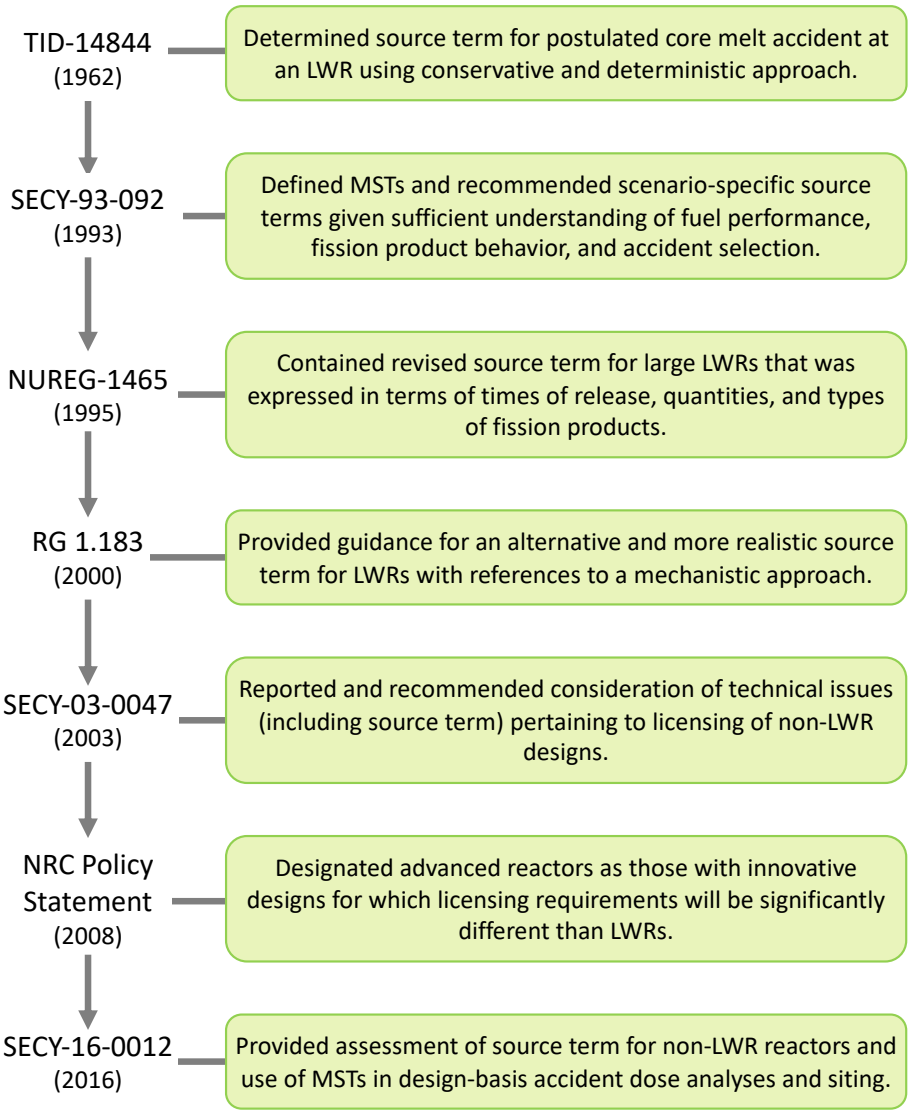


**Figure 3**. NRC documents related to mechanistic source term analysis (from SECY-16-0012 and Grabaskas et al., 2015).

### *2.1 Light Water Reactors*

In 1962, the U.S. Atomic Energy Commission (AEC)—predecessor to the NRC—published the technical information document "Calculation of Distance Factors for Power and Test Reactors" (TID-14844). This document detailed the release of fission products from the core to the reactor containment during a postulated accident involving "substantial meltdown" of the core. The source term analysis described therein used conservative bounding assumptions for a maximum credible accident in an LWR (Table 1). The information in Table 1 was derived from experiments on irradiated uranium oxide pellets performed in the 1950s and is not related to any phenomenological processes. The analysis in TID-14844 was incorporated into the Regulatory Guide (R.G.) 1.3 (NRC, 1974a) and R.G. 1.4 (NRC, 1974b) and has historically been the reference for determining compliance with the NRC's reactor site criteria (10 CFR § 100) and other plant performance requirements.

**Table 1.** Key Assumptions from TID-14844 Source Term (adapted from Grabaskas et al., 2015).

| Parameter | Assumptions |
|---|---|
| Accident sequence | Maximum credible accident for LWR: pipe rupture resulting in massive core melt |
| Release to containment | Noble gases: 100%<br>Halogens: 50%<br>Remaining solids: 1% |
| Containment leakage rate | Maximum allowable: 0.1% per day |
| Engineered safety features | No credit |
| Release period | Instantaneous |

The source term described in TID-14844 took an overly conservative and simplistic approach due to a lack of information on the chemical and physical processes that can occur during LWR operation and postulated accident scenarios. For example, radionuclides were assumed to be instantaneously released to containment. More realistic models are required for a source term analysis to provide useful feedback into the reactor design process and to justify the size of reactor site emergency planning zones. Considering the significant progress in the technical understanding of reactor accident behavior for LWRs since TID-14844 was issued, the NRC recognized in the early 1990s the need for and feasibility of a mechanistic approach to source term and released SECY-93-092 as a result.

Instead of using a bounding accident approach, MSTs consider the real transport and retention processes, use fundamental chemistry knowledge, and consider the effects of barriers to release (Jerden et al., 2019a). Unrealistic guidance provided by a conservative bounding source term approach could promote decisions that negatively impact safety. This shortcoming led to the release of NUREG-1465 in 1995, which documented a revised source term for a range of specific accident scenarios and served as a basis for revisions to regulatory requirements for existing and future LWRs. New considerations detailed in NUREG-1465 included specific fuel failure phenomena, in-containment retention mechanisms, fission product removal using engineered safety features, and uncertainty in quantitative terms.

Issued in 2000, R.G. 1.183 “Alternative Radiological Source Terms for Evaluating Design Basis Accidents at Nuclear Power Reactors” was based on the guidance provided in NUREG-1465. It is specific to LWRs and considers one source term for all PWRs and another source term for all BWRs. The alternative source term deterministically assumes a failure of core cooling accident scenario, which is similar to TID-14844. However, it mechanistically models accident progression and time-dependent release to containment.

The fraction, onset, and duration of radionuclide release from the reactor core for the PWR and BWR source term in R.G. 1.183 is shown in Table 2. The gap release phase refers to radionuclide release from the fuel-cladding gap at the onset of fuel failure and is immediately followed by the early in-vessel phase (i.e., radionuclide release prior to vessel failure). Only these first two phases of release progression are considered because they are assumed to make up the worst two hours of the accident (10 CFR § 50.67 Accident Source Term). The guidance in R.G. 1.183 was only to be followed if the licensee could meet specified criteria for an acceptable alternative source term. Otherwise, R.G 1.3 and R.G. 1.4 were to be used.

**Table 2** Release fractions to containment from R.G. 1.183 (adapted from Grabaskas et al., 2015).

| | BWR | | PWR | |
|---|---|---|---|---|
| | Gap Release | Early In-vessel | Gap Release | Early In-vessel |
| **Onset (s)** | **120** | **1800** | **30** | **1800** |
| **Duration (h)** | **0.5** | **1.5** | **0.5** | **1.3** |
| Noble gases | 0.05 | 0.95 | 0.05 | 0.95 |
| Halogens | 0.05 | 0.25 | 0.05 | 0.35 |
| Alkali metals | 0.05 | 0.20 | 0.05 | 0.25 |
| Tellurium group | 0 | 0.05 | 0 | 0.05 |
| Barium, strontium | 0 | 0.02 | 0 | 0.02 |
| Noble metals | 0 | 0.0025 | 0 | 0.0025 |
| Cerium group | 0 | 0.0005 | 0 | 0.0005 |
| Lanthanides | 0 | 0.0002 | 0 | 0.0002 |

### *2.2 Advanced, Non-LWR Reactors*

The guidance inspired by TID-14844 and promulgated in R.G. 1.183 was explicitly for LWRs due to their historical prevalence. By definition, designs of advanced reactors differ significantly from LWRs, and thus, source term approaches historically applied to LWRs are not necessarily appropriate for MSRs. For example, the MCA described in TID-14844 was a loss of coolant accident (LOCA) that is not a realistic MCA for some advanced reactor designs (e.g., sodium fast reactor; Grabaskas et al., 2015). Considering the interest from advanced reactor vendors during preliminary licensing talks in the early 1990s, the NRC formally addressed the need to develop an MST approach for reactor licensing with the issuance of SECY-93-092 and affirmed their approval for the use of MSTs in licensing decisions related to containment and siting in SECY-03-0047. Therein, NRC staff noted that MST use would be effort-intensive but necessary to accommodate unique advanced reactor designs that could affect source term.

With the establishment of the Next Generation Nuclear Plant (NGNP) Project under the Energy Policy Act (EPAct) in 2005, the DOE and Idaho National Laboratory (INL) were tasked with developing the licensing application, including an MST, for the modular high-temperature gas-cooled reactor (MHTGR). In a white paper submitted to the NRC, the DOE/INL outlined their anticipated approach for developing an MST for MHTGRs that is generic enough for both possible fuel types (pebble bed and prismatic block) and proposed an MST for each license basis event (INL, 2010). The white paper sought feedback from the NRC on the following issues:

> Issue 1: *"Agreement that the definition of event specific mechanistic source terms for the HTGR is acceptable."*
>
> Issue 2: *"Agreement that the approach to calculating event-specific mechanistic source terms for the HTGR technology is acceptable, subject to validation of the design methods and supporting data that form the bases of the calculations."*
>
> Issue 3: *"Agreement on the acceptability of the approach of the planned fission product transport tests of the NGNP/Advanced Gas Reactor (AGR) Fuel Development and Qualification Program, as supplemented by the existing irradiation and post-irradiation heating data bases, to validate these fission product transport analytical tools."*

The approach referred to in Issue 2 is an analysis of several barriers of functional containment that limit the release of radionuclides to the environment for each postulated event under normal operating conditions, abnormal operations conditions, and accident conditions. Specifically, DOE/INL proposed detailed methods for quantifying key factors:

- the generation and transport of each radiologically significant species of fission product from the fuel kernel to the reactor coolant,
- the concentration and form of each radiologically significant chemical species in the helium primary circuit during normal operations,
- the concentration and form of each radiologically significant chemical species in helium released during depressurization events, and
- the effects of radionuclide form, condensation, settling, vent-path configuration, and vent filtering on the time-dependent transport of radionuclides through the reactor building and to the atmosphere for each postulated event.

In their most recent response to the DOE/INL, the NRC staff concluded that the proposed methodology for generating an MST for MHTGRs is in alignment with the staff's current position on the treatment of advanced reactor MSTs, with caveats (NRC, 2014). The NRC suggested that, in addition to considering licensing basis events, the DOE/INL should also include bounding events such as those identified in NUREG-1338 in their MST approach. In general, the NRC's main regulatory concerns appear to be related to the development and validation of models that can accurately represent the phenomenological behavior of fission product generation and transport. Uncertainty evaluation is crucial to bound aspects of accident consequences when there is a lack of operating and experimental data.

To provide clarity to advanced reactor-related decision making, the American Society of Mechanical Engineers (ASME) and the American Nuclear Society (ANS) released the technology-neutral standard "Probabilistic Risk Assessment Standard for advanced Non-LWR Nuclear Power Plants" in 2013. This lists several qualitative objectives and high-level requirements for an MST analysis for advanced reactors.

Six objectives for an MST analysis are (ASME/ANS 2013):

- *"Identification of inventories available for release within the reactor coolant system pressure boundary,*
- *Identification and characterization of the phenomena affecting radionuclide transport,*
- *Definition of reactor-specific release categories for use in end state and event sequence grouping,*
- *Determination of release parameters (e.g. chemical phase, release timing and duration, etc.),*
- *Identification and evaluation of relevant uncertainties, and*
- *Documentation of the mechanistic analysis."*

Five high-level requirements are (ASME/ANS 2013):

- *"Release categories shall be defined for defining event sequence end states and for grouping event sequences and event sequence families with the same or similar mechanistic source terms.*
- *The mechanistic source term analysis shall include a method for determining the mechanistic source term for each release category.*
- *The mechanistic source term analysis shall include calculations to quantitatively characterize the mechanistic source terms for each release category.*
- *Uncertainties in the mechanistic source terms and associated radionuclide transport phenomena shall be characterized and quantified to the extent practical. Key sources of model uncertainty and assumptions shall be identified, and their potential impact on the results shall be understood. Those sources of uncertainty that are not quantified shall be addressed via sensitivity analysis.*
- *The mechanistic source term analysis shall be documented consistent with the applicable supporting requirements."*

Following the recommendations provided by ASME/ANS, the NRC released SECY-16-0012 in 2016, "Accident Source Terms and Siting for SMRs and Non-LWRs", which discussed the issues associated with using MSTs in design-basis accident dose analyses and siting. Therein, NRC staff stated that venders could use MSTs in the licensing application for non-LWR designs, given the availability of tools and data for an adequate analysis. Another focus of the document was that MST use in a license application could lead to reduced exclusion area boundaries and closer proximity to population centers for certain advanced reactors. For example, small modular reactors (SMRs) that contain smaller amounts of fuel and utilize passive safety design features are expected to have smaller source terms than LWRs.

To date, six advanced non-LWR reactor designers have formally notified the NRC that they intend to engage in regulatory interactions. The range of reactor technologies in this initial set of advanced, non-LWR designs indicates the need for a generic source term approach that can address specific aspects of individual designs. A mechanistic source term approach was recently demonstrated for a generic metal fueled sodium fast reactor concept (Grabaskas et al., 2016a) that can inform future advanced reactor source term developments. The major challenges for developing an MST approach for non-LWR advanced reactor designs will likely be the need for new modeling tools, alteration modifications of existing codes, and an extensive experimental program to obtain necessary thermochemical and thermophysical data (Jerden et al., 2019a).

**Table 3.** Summary of non-LWR reactor designers that are formally interacting with NRC[a].

| Developer | Pre-application information | Technology |
|---|---|---|
| General Atomics | General Atomics | Helium-Cooled Fast Reactor |
| X-Energy LLC | XE-100 | Modular High Temperature Gas-Cooled Reactor |
| Kairos Power LLC | Kairos Power Fluoride Salt-Cooled, High Temperature Reactor (KP-FHR) | Molten Salt Reactor |
| Terrestrial Energy USA Ltd | Integral Molten Salt Reactor (IMSR) | Molten Salt Reactor |
| TerraPower, LLC | Molten Chloride Fast Reactor (MCFR) | Molten Salt Reactor |
| Westinghouse Electric Company | eVinci | Micro Reactor |

[a] *Information from https://www.nrc.gov/reactors/new-reactors/advanced.html#advRxWs*

# 3 Radionuclide Sources in MSRs: Inventory Distribution During Normal Operation

This section provides information addressing the first objective in Figure 1: identify and characterize radionuclide sources. This information will be needed as part of an MSR MST to justify the assumed initial states (starting distribution of radionuclides) for the hypothetical accident scenarios identified in Section 1. The MST approach being developed will be technology-inclusive and radionuclide distribution processes for both fluoride and chloride fueled reactors will be considered.

Throughout this report, we refer to the molten salt reactor experiment (MSRE), the molten salt breeder reactor (MSBR), and the molten salt demonstration reactor (MSDR). These projects were the culmination of years of research on molten salt fueled reactors performed at Oak Ridge National Laboratory (ORNL), which started as an investigation of MSR technology for powering aircraft (1950s) (e.g., Ergen et al., 1957). The Aircraft Reactor Program led to the testing of a high temperature (up to 860 ºC) MSR core fueled by high enriched uranium dissolved in a NaF-$ZrF_4$ eutectic salt. The MSRE used a 7.3 MWt reactor operated at ORNL from 1965 – 1969 as a demonstration of the technology needed to develop the commercial large scale (2250 MWt) MSBR. In the 1970s, the MSDR concept was developed as a more moderate (750 MWt) semi-commercial alternative to the MSBR (Bettis et al., 1972). The fuel types and characteristics of the MSRE, MSBR, and MSDR are summarized in Table 4.

**Table 4.** Basic characteristics of the molten salt reactor experiment, the molten salt breeder reactor and the molten salt demonstration reactor.

| | **MSRE** | **MSBR** | **MSDR** |
|---|---|---|---|
| Power (MWt) | 7.3 | 2250 | 750 |
| Fuel Salt (mol %) | | | |
| LiF | 65 | 71.7 | 71.5 |
| $BeF_2$ | 29.1 | 16 | 16 |
| $ThF_4$ | none | 12 | 12 |
| $UF_4$ | 0.9 | 0.3 | 0.5 |
| $ZrF_4$ | 5 | none | none |
| Core Inlet T (ºC) | 632 | 566 | 677 |
| Core Outlet T (ºC) | 654 | 704 | 566 |
| Average power density of fuel salt ($MW/cm^3$) | 4 | 46 | 46 |
| Coolant Salt | LiF-$BeF_2$ | $NaBF_4$-NaF | LiF-$BeF_2$ |

## *3.1 Fission Yields*

The full array of fission products will be produced within the fuel salt of an MSR. The concentration of any isotope will depend on the balance between the rate of production by fission and the rate of destruction by decay. Isotopes in the salt reactor system will be produced as direct products of fission and by neutron absorption by lighter elements. The fission yields and decay rates of the key isotopes considered in the MSRE project are shown in Table 5 (adapted from Compere et al., 1975). The actual fission product inventory at any time will vary with reactor power (which my change on a weekly basis) and the fissile composition of the fuel (i.e., the ratios of $^{233}U/^{235}U/^{239}Pu$).

The calculated elemental fission product inventory for MSRE $^{235}U$ operation is summarized in Figure 4. This inventory was calculated by Bell, 1972 using ORIGEN for a reactor power of 4.18 MW, a flux of

$2.35 \times 10^{12}$ N/($cm^2$ s), and a burnup of 2983 MWd, assuming the continuous stripping of Xe and Kr gases from the core.

**Table 5.** Fission yields for some key radionuclides (adapted from Compere et al., 1975).

| | | | Cumulative fission yield[a] | | |
|---|---|---|---|---|---|
| **Chain** | **Isotope** | **Half-Life** (days) | **$^{233}$U** | **$^{235}$U** | **$^{239}$Pu** |
| 89 | Sr | 52 | 5.86 | 4.79 | 1.711 |
| 90 | Sr | 1.0E+04 | 6.43 | 5.77 | 2.21 |
| 91 | Sr | 0.4 | 5.57 | 5.81 | 2.43 |
| 91 | Y | 59 | 5.57 | 5.81 | 2.43 |
| 95 | Zr | 65 | 6.05 | 6.2 | 4.97 |
| 95 | Nb | 35 | 6.05 | 6.2 | 4.97 |
| 99 | Mo | 2.79 | 4.8 | 6.06 | 6.1 |
| 99 | Tc | 7.7E+07 | 4.8 | 6.06 | 6.1 |
| 103 | Ru | 39.5 | 1.8 | 3 | 5.67 |
| 106 | Ru | 368 | 0.24 | 0.38 | 4.57 |
| 110 | Ag(m)[b] | 253 | — | — | — |
| 111 | Ag | 7.5 | 0.0242 | 0.0192 | 0.232 |
| 125 | Sb | 985.5 | 0.084 | 0.021 | 0.115 |
| 127 | Te(m) | 100 | 0.6 | 0.13 | 0.39 |
| 129 | Te(m) | 34 | 2 | 0.8 | 2 |
| 131 | I | 8.05 | 2.9 | 2.93 | 3.78 |
| 132 | Te | 3.25 | 4.4 | 4.24 | 5.1 |
| 134 | Cs[b] | 750 | — | — | — |
| 135 | Xe | 0.38 | 6.16 | 6.41 | 7.17 |
| 137 | Cs | 1.1E+04 | 6.58 | 6.15 | 6.63 |
| 140 | Ba | 12.8 | 5.4 | 6.85 | 5.56 |
| 141 | Ce | 32.3 | 6.49 | 6.4 | 5.01 |
| 141 | Ce | 32.5 | 6.49 | 6.4 | 5.09 |
| 143 | Pr | 13.57 | 6 | 5.73 | 4.56 |
| 144 | Ce | 284 | 4.61 | 5.62 | 3.93 |
| 147 | Nd | 11.1 | 1.98 | 2.36 | 2.07 |
| 147 | Pm | 967.25 | 1.98 | 2.36 | 2.07 |
| 147 | Pm | 949 | 1.98 | 2.36 | 2.07 |
| 148 | Pm | 5.36 | 1.34 | 1.71 | 1.73 |
| 149 | Pm | 2.21 | 0.76 | 1.13 | 1.32 |
| 151 | Sm | 3.2E+04 | 0.34 | 0.44 | 0.8 |
| 155 | Eu | 1.7E+03 | 0.02 | 0.03 | 0.23 |

[a]Fission yields given as atoms produced per 100 atoms of fissile isotope.
[b]Yield values for $^{110(m)}$Ag and $^{134}$Cs are not shown because these isotopes are produced by neutron absorption by lighter chain nuclides.

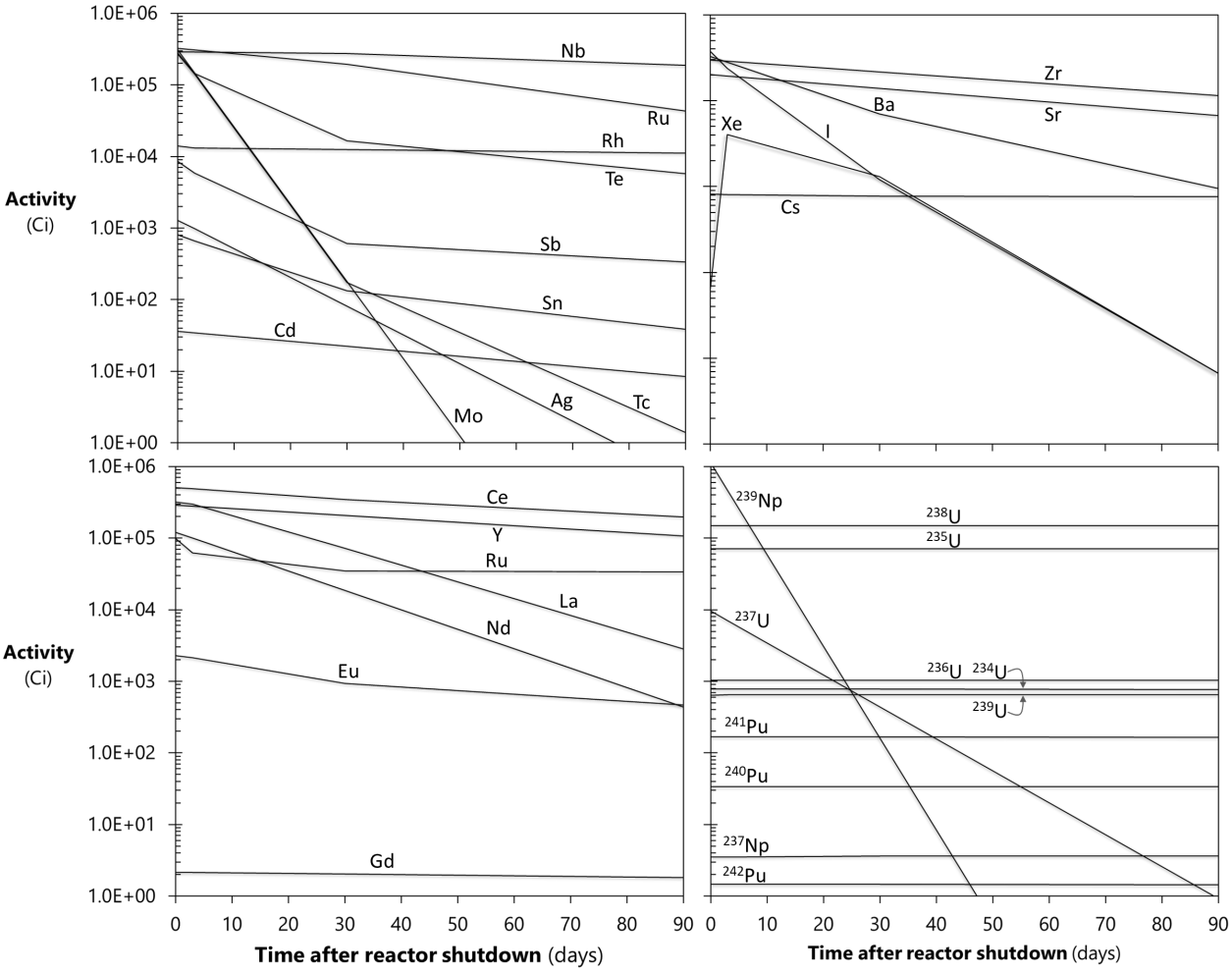


**Figure 4.** Calculated fission product activities for the MSRE (plotted from tabulated results of Bell, 1972).

Taube, 1978 gives an example of the projected fission product inventory for a 2000 MW(t) chloride fueled fast breeder reactor containing a mixture of 15 mol % $PuCl_3$ + 85 mol % NaCl as the fuel and a fertile blanket salt consisting of 65 mol % $^{238}UCl_3$ + 35 mol % NaCl. The elemental fission yields for this system are shown in Table 6. This table also gives the predicted valence state and chloride chemical compatibility.

**Table 6.** Fission yields for $^{239}PuCl_3$/NaCl and $^{235}UCl_3$/NaCl fueled fast spectrum MSR (yields per 100 atoms of $^{239}Pu$ fission for 10-day irradiation). Adapted from Taube, 1971 and Burris and Dillon, 1957.

| Element | $^{238}Pu$ Yield | $^{235}U$ Yield | Oxidation State | Chloride Species |
|---|---|---|---|---|
| Br | 0.003 | 0.142 | 0 | none |
| I | 6.177 | 4.014 | 0 | none |
| Kr | 0.942 | 3.021 | 0 | none |
| Pd | 12.657 | 1.31 | 0 | none |
| Rh | 1.736 | 0.557 | 0 | none |
| Ru | 31.445 | 18.265 | 0 | none |
| Se | 0.008 | 0.396 | 0 | none |
| Tc | 4.014 | 4.217 | 0 | none |
| Xe | 21.234 | 21.793 | 0 | none |
| Ag | 1.88 | 0.125 | +1 | AgCl |
| Cs | 13.355 | 14.161 | +1 | CsCl |
| In | 0.06 | 0.029 | +1 | InCl |
| Rb | 1.05 | 3.723 | +1 | RbCl |
| Ba | 9.502 | 10.642 | +2 | $BaCl_2$ |
| Cd | 0.66 | 0.206 | +2 | $CdCl_2$ |
| Mo | 18.16 | 20.857 | +2 | $MoCl_2$ |
| Sn | 0.324 | 0.388 | +2 | $SnCl_2$ |
| Sr | 5.487 | 12.176 | +2 | $SrCl_2$ |
| Te | 7.654 | 4.251 | +2 | $TeCl_2$ |
| Ce | 13.986 | 16.112 | +3 | $CeCl_3$ |
| Eu | 0.595 | 0.144 | +3 | $EuCl_3$ |
| Gd | 0.028 | 0.007 | +3 | $GdCl_3$ |
| La | 5.79 | 6.808 | +3 | $LaCl_3$ |
| Nd | 11.87 | 13.626 | +3 | $NdCl_3$ |
| Pm | 1.44 | 1.249 | +3 | $PmCl_3$ |
| Pr | 4.278 | 5.029 | +3 | $PrCl_3$ |
| Sb | 0.674 | 0.339 | +3 | $SbCl_3$ |
| Sm | 3.737 | 1.592 | +3 | $SmCl_3$ |
| Y | 3.028 | 5.71 | +3 | $YCl_3$ |
| Zr | 21.52 | 29.732 | +4 | $ZrCl_3$ |
| Nb | 0.289 | 0.37 | +5 | $NbCl_5$ |

An example actinide inventory for a molten chloride fast reactor is shown in Table 7. This table is based on the REBUS concept that is powered by a $UCl_3$+transuranic (TRU) fuel mixture of 45 mol % (U + 15.6 atom % TRU)$Cl_3$ + 55 mol % NaCl (Mourogov and Bokov, 2006).

**Table 7.** Transuranic isotopic composition of the REBUS fast spectrum MSR fueled with 45 mol % (U,TRU)$Cl_3$ + 55 mol % NaCl (Mourogov and Bokov, 2006).

| Isotopes | Initial Composition (atom % of TRU) | Equilibrium Composition (atom % TRU) |
|---|---|---|
| $^{238}$Pu | 2.13 | 2.23 |
| $^{239}$Pu | 48.33 | 58.02 |
| $^{240}$Pu | 22.17 | 27.63 |
| $^{241}$Pu | 9.05 | 3.35 |
| $^{242}$Pu | 6.38 | 4.05 |
| $^{237}$Np | 4.8 | 0.65 |
| $^{239}$Np | 0 | 0.07 |
| $^{241}$Am | 5.17 | 1.5 |
| $^{242m}$Am | 0.01 | 0.12 |
| $^{243}$Am | 1.48 | 1.05 |
| $^{242}$Cm | 0 | 0.07 |
| $^{243}$Cm | 0 | 0.01 |
| $^{244}$Cm | 0.43 | 1.02 |
| $^{245}$Cm | 0.04 | 0.19 |
| $^{246}$Cm | 0 | 0.05 |

As shown above, the fission products yields for both $^{235}$U and $^{239}$Pu indicate the fission products Zr, Ru, Xe, Mo, Ce, Cs, Pd, Nd, Ba, Te, I, La, Sr, Pr, Tc and Nb will be the most abundant on both mass and activity bases (Table 5, Table 6, and Figure 4).

### *3.2 Radiotoxicity: Identification of Major Dose Contributors to Prioritize Chemical Model Development*

The ranking of radionuclides in terms of radiotoxicity allows for the prioritization of particular chemical systems for both experimental and model development work. The U.S. EPA defined three measures of radiotoxicity that may be used in the control of internal exposure to radionuclides in the workplace. These measures are the annual limit on intake (ALI), the derived air concentration (DAC) and the effective dose equivalent conversion factor that quantifies the absorbed dose to tissues and organs for specific isotopes (Eckerman et al., 1988). The DAC is defined as the concentration of a radionuclide in air which, if breathed for a work-year, would result in an intake corresponding to the ALI of that radionuclide (Eckerman et al., 1988). DAC values are used for limiting radionuclide intake through breathing of contaminated air and ALIs are used for assessing doses due to accidental ingestion of radionuclides. The ALI and DAC values are derived from stochastic and non-stochastic effects of radioactive dose to organs due to radionuclide inhalation or ingestion. The relative organ damage caused by various radionuclides is quantified by the dose equivalent factor (Eckerman et al., 1988).

Table 8 and Table 9 rank the major fission products and actinides (respectively) in terms of the dose equivalent factor and show the ALI and DAC values for each isotope. The relative radiotoxicity derived from these values is plotted in Figure 5. From a radiotoxicity perspective, the ten most important fission products within the MSR fuel salts will be Cs, I, Sr, Ru, Ce, Cd, Sn, Y, Te, and Ba (Table 8 and Figure 5). All of the major actinides (U, Pu, Th, Np, Am, Cm) have nuclides that are, in general, considerably more radiotoxic than the fission products (Table 9 and Figure 5).

**Table 8**. Fission product radionuclides ranked in terms of radiotoxicity as quantified by the U.S. EPA annual limit on intake (ALI) and derived air concentration (DAC) and effective dose equivalent conversion factor (Dose Factor) from Eckerman et al., 1988.

| Element | Mass Number | Half Life (days) | $^{235}$U Yield | Dose Factor[a] (mrem/mCi) | DAC (MBq/m$^3$) | Inhalation ALI (MBq) | Ingestion ALI (MBq) |
|---|---|---|---|---|---|---|---|
| Cs | 135 | 7.7E+08 | 6.361 | 706.7 | 2.0E-02 | 40 | 30 |
| I | 129 | 6.2E+09 | 0.671 | 276.0 | 1.0E-04 | 0.3 | 0.2 |
| Sr | 90 | 1.0E+04 | 4.420 | 142.5 | 3.0E-04 | 0.7 | 1 |
| I | 131 | 8.0E+00 | 1.102 | 53.3 | 7.0E-04 | 2 | 1 |
| Cs | 137 | 9.9E+03 | 5.790 | 50.0 | 2.0E-03 | 6 | 4 |
| Ru | 106 | 3.7E+02 | 0.454 | 27.4 | 1.0E-03 | 3 | 7 |
| Ce | 144 | 2.8E+02 | 4.650 | 21.0 | 4.0E-04 | 0.9 | 8 |
| Cd | 115m | 4.3E+01 | 0.004 | 16.2 | 8.0E-04 | 2 | 10 |
| Sn | 125 | 9.4E+00 | 0.026 | 12.3 | 1.0E-02 | 30 | 10 |
| Y | 90 | 2.5E+00 | 0.001 | 10.8 | 3.0E-03 | 30 | 20 |
| Te | 129m | 3.4E+01 | 0.112 | 10.7 | 1.0E-02 | 20 | 20 |
| I | 133 | 2.7E-01 | 0.273 | 10.4 | 4.0E-03 | 10 | 5 |
| Y | 91 | 5.7E+01 | 4.360 | 9.5 | 4.0E+00 | 9000 | 20 |
| Ba | 140 | 1.3E+01 | 2.909 | 9.5 | 2.0E-02 | 50 | 20 |
| Te | 132 | 3.2E+00 | 0.690 | 9.4 | 4.0E-03 | 9 | 8 |
| Sr | 89 | 5.3E+01 | 3.465 | 9.3 | 1.0E-02 | 30 | 20 |
| Eu | 156 | 1.5E+01 | 0.007 | 9.2 | 7.0E-03 | 20 | 20 |
| Se | 79 | 2.4E+07 | 0.042 | 8.7 | 1.0E-02 | 30 | 20 |
| La | 140 | 1.7E+00 | 0.361 | 8.4 | 2.0E-02 | 50 | 20 |
| Te | 127m | 1.2E+02 | 0.032 | 8.3 | 4.0E-03 | 10 | 20 |
| Ag | 111 | 7.6E+00 | 0.023 | 5.1 | 2.0E-02 | 60 | 30 |
| Rb | 87 | 2.2E+13 | 2.879 | 4.9 | 2.0E-02 | 60 | 40 |
| Pr | 143 | 1.4E+01 | 2.505 | 4.7 | 1.0E-02 | 30 | 30 |
| Y | 93 | 4.2E-01 | 0.108 | 4.6 | 4.0E-02 | 100 | 40 |
| Sb | 127 | 3.9E+00 | 0.048 | 4.4 | 3.0E-02 | 80 | 30 |
| Nd | 147 | 1.1E+01 | 1.478 | 4.4 | 1.0E-02 | 30 | 40 |
| Pm | 149 | 2.3E+00 | 0.129 | 4.0 | 3.0E-02 | 70 | 40 |
| Zr | 95 | 6.5E+01 | 5.790 | 3.8 | 2.0E-03 | 5 | 50 |
| Ru | 103 | 4.0E+01 | 3.125 | 3.0 | 3.0E-02 | 60 | 70 |
| Mo | 99 | 2.8E+00 | 0.832 | 3.0 | 4.0E-02 | 100 | 60 |
| Cl | 36 | 1.1E+08 | ---- | 3.0 | 4.0E-02 | 90 | 60 |
| Ce | 141 | 3.3E+01 | 3.858 | 2.9 | 1.0E-02 | 30 | 60 |
| Sb | 125 | 9.9E+02 | 0.097 | 2.8 | 4.0E-02 | 90 | 80 |
| Nb | 95 | 3.5E+01 | 0.797 | 2.6 | 2.0E-02 | 50 | 80 |
| Sr | 91 | 4.0E-01 | 0.014 | 2.5 | 9.0E-02 | 200 | 80 |
| Zr | 93 | 3.5E+08 | 5.317 | 1.7 | 1.0E-04 | 0.2 | 50 |
| Eu | 155 | 6.2E+02 | 0.029 | 1.5 | 1.0E-03 | 3 | 100 |
| Rh | 105 | 3.7E+01 | 0.075 | 1.5 | 2.0E-01 | 400 | 100 |
| Tc | 99 | 7.7E+07 | 5.303 | 1.5 | 8.0E-02 | 200 | 100 |
| Sn | 119m | 2.5E+02 | 0.052 | 1.4 | 4.0E-02 | 90 | 100 |
| Sn | 117m | 1.4E+01 | 0.027 | 1.2 | 2.0E-02 | 50 | 60 |
| Pm | 147 | 9.5E+02 | 1.748 | 1.0 | 2.0E-03 | 5 | 200 |
| Sn | 121 | 1.1E+00 | 0.002 | 0.9 | 2.0E-01 | 600 | 200 |
| Sm | 151 | 3.0E+00 | 0.438 | 0.4 | 2.0E-03 | 4 | 500 |
| Pd | 107 | 2.6E+09 | 0.280 | 0.1 | 3.0E-01 | 800 | 1000 |
| Br | 83 | 9.7E-02 | 0.002 | 0.1 | 1.0E+00 | 2000 | 2000 |
| H | 3 | 4.5E+03 | — | 0.1 | 8.0E-01 | 3000 | 3000 |
| Tc | 99m | 2.5E-01 | 0.065 | 0.1 | 2.0E+00 | 6000 | 3000 |
| Kr | 85 | 3.4E+03 | 0.264 | — | 5.0E+00 | — | — |
| Kr | 85m | 1.8E-01 | 0.010 | — | 8.0E-01 | — | — |
| Xe | 133 | 5.3E+00 | 1.665 | — | 4.0E+00 | — | — |
| Xe | 135 | 3.8E-01 | 0.110 | — | 5.0E-01 | — | — |

[a] Dose Factor = the effective dose equivalent which utilizes a weighted sum of doses to all irradiated organs and tissues.

**Table 9.** Actinides and thorium decay chain nuclides ranked in terms of radiotoxicity as quantified by the U.S. EPA annual limit on intake (ALI) and derived air concentration (DAC) and effective dose equivalent conversion factor (Dose Factor) from Eckerman et al., 1988.

| Element | Mass Number | Half Life (years) | Dose Factor[a] (mrem/mCi) | DAC (MBq/m3) | Inhalation ALI (MBq) | Ingestion ALI (MBq) |
|---|---|---|---|---|---|---|
| Np | 237 | 2.1E+06 | 4440.0 | 6.0E-08 | 2.0E-04 | 0.02 |
| Cm | 245 | 5.8E+03 | 3737.0 | 9.0E-08 | 2.0E-04 | 0.03 |
| Cm | 246 | 4.7E+03 | 3700.0 | 9.0E-08 | 2.0E-04 | 0.03 |
| Am | 241 | 4.3E+02 | 3640.8 | 1.0E-07 | 2.0E-04 | 0.03 |
| Am | 243 | 7.4E+03 | 3622.3 | 1.0E-07 | 2.0E-04 | 0.03 |
| Pu | 239 | 2.4E+04 | 3537.2 | 1.0E-07 | 2.0E-04 | 0.03 |
| Pu | 240 | 6.5E+03 | 3537.2 | 1.0E-07 | 2.0E-04 | 0.03 |
| Am | 242(m) | 1.5E+02 | 3515.0 | 1.0E-07 | 2.0E-04 | 0.03 |
| Pu | 242 | 3.8E+05 | 3359.6 | 1.0E-07 | 2.0E-04 | 0.03 |
| Pu | 238 | 8.8E+01 | 3200.5 | 1.0E-07 | 3.0E-04 | 0.03 |
| Cm | 242 | 162.8 (*days*) | 2512.3 | 4.0E-06 | 1.0E-02 | 1 |
| Cm | 243 | 2.9E+01 | 2512.3 | 1.0E-07 | 3.0E-04 | 0.04 |
| Cm | 244 | 1.8E+01 | 2016.5 | 2.0E-07 | 4.0E-04 | 0.05 |
| U | 234 | 2.4E+05 | 283.4 | 2.0E-05 | 5.0E-02 | 0.4 |
| U | 236 | 2.3E+07 | 268.6 | 2.0E-05 | 5.0E-02 | 0.5 |
| U | 235 | 7.0E+08 | 266.0 | 2.0E-05 | 5.0E-02 | 0.5 |
| U | 238 | 4.5E+09 | 254.6 | 2.0E-05 | 5.0E-02 | 0.5 |
| Pu | 241 | 1.4E+01 | 68.5 | 5.0E-06 | 1.0E-02 | 1 |
| Np | 239 | 2.355 (*days*) | 3.3 | 1.0E-03 | 2.0E+00 | 60 |
| U | 237 | 6.75 (*days*) | 3.1 | 4.0E-02 | 1.0E+02 | 60 |
| *Prominent thorium fuel cycle nuclides* | | | | | | |
| Th | 232 | 1.4E+10 | 2730.6 | 2.0E-08 | 4.0E-05 | 0.03 |
| U | 233 | 1.6E+05 | 1309.8 | 2.0E-05 | 4.0E-02 | 0.4 |
| Th | 228 | 1.9E+00 | 395.9 | 3.0E-07 | 4.0E-04 | 0.2 |
| Ra | 224 | 3.66 (days) | 365.9 | 3.0E-05 | 6.0E-02 | 0.3 |
| U | 232 | 7.2E+01 | 289.0 | 3.0E-06 | 8.0E-03 | 0.08 |
| Pa | 233 | 27 (*days*) | 3.6 | 1.0E-02 | 3.0E+01 | 50 |

[a] Dose Factor = the effective dose equivalent which utilizes a weighted sum of doses to all irradiated organs and tissues.

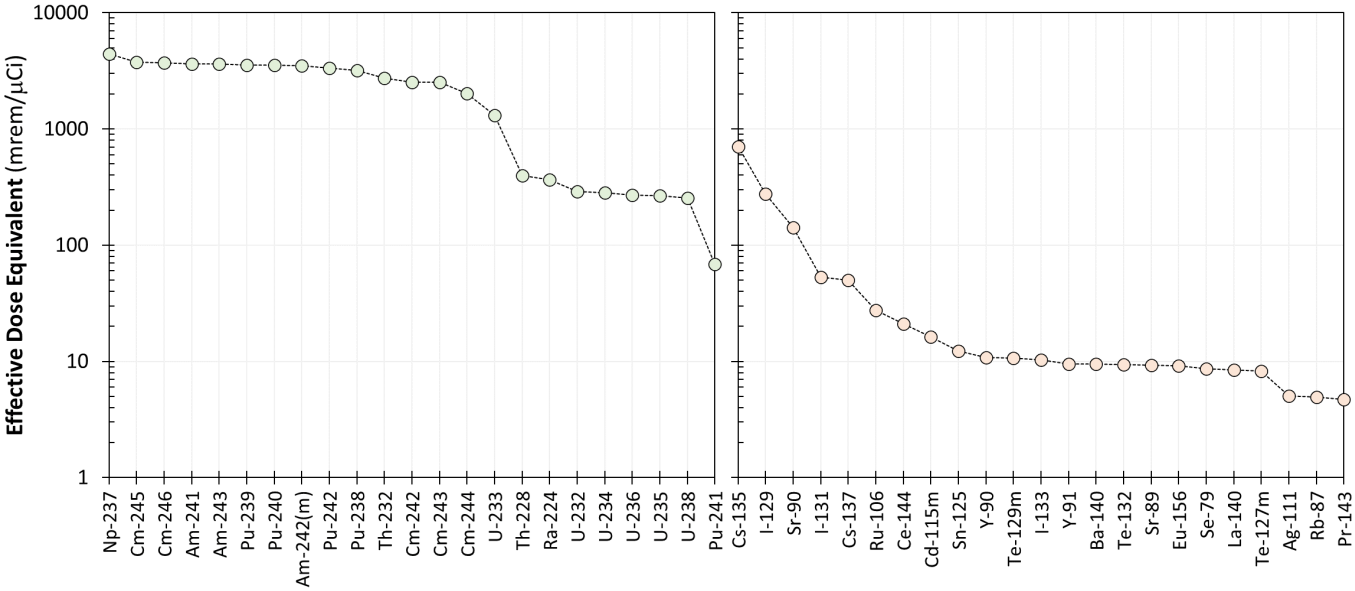


**Figure 5.** Actinides and fission products ranked by radiotoxicity as quantified by the effective dose equivalent (plotted from tabulated values of Eckerman et al., 1988).

### *3.3 Inventory Distribution Based on Chemical Affinity during Normal Operation*

Observations from the MSRE project led to the sorting of fission products into three categories: salt-seeking elements, noble elements and volatile elements. As shown in Figure 6, salt seeking elements include Rb, Sr, Y, Zr, Cs, Ba, La, Ce and the lanthanides and noble acting elements include Nb, Mo, Tc, Ru, Rh, Pd, Ag, Sb, Te and possibly Cd, In and Sn. It should be noted that Nb may act as a salt seeking or noble acting element depending on the redox conditions of the fuel. Iodine can form iodides that remain in the salt but could also volatilize as $I_2$ if the salt redox potential increases significantly above the optimal operating conditions (for example due to an oxygen-bearing gas contacting the fuel). The disposition of some important elements will depend on their precursors. For example, some isotopes of Rb, Sr, Y, Cs, and Ba that are important to source term have noble-gas progenitors with half-lives long enough to enable their escape into the cover gas before decaying (Figure 7). This could lead to an accumulation of some key source term radionuclides in the off-gas system. Similarly, the precursor of $^{131}I$ is $^{131}Te$ and iodine will be produced in locations where tellurium has been deposited (for example on metal surfaces or within the off-gas system).

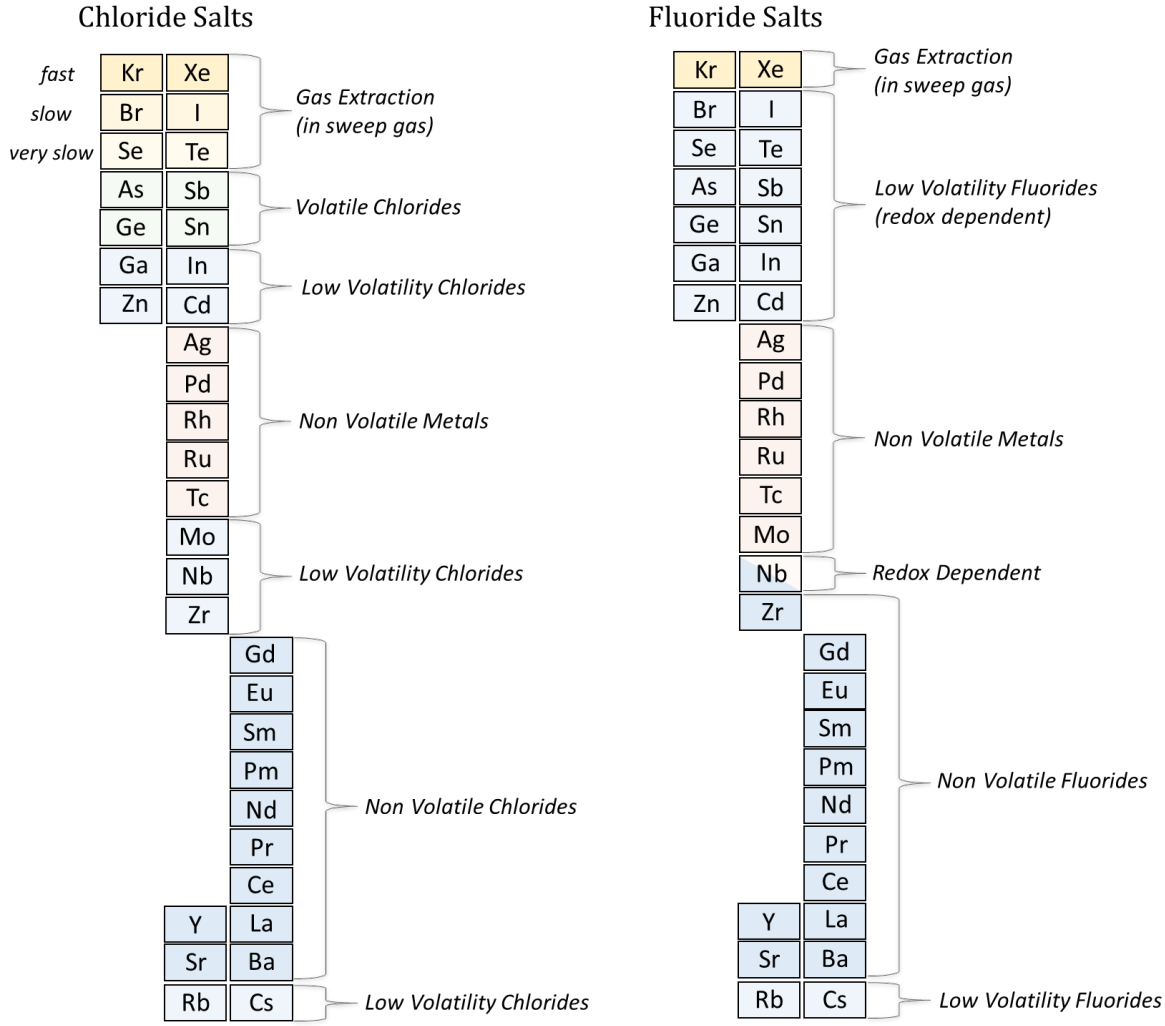


**Figure 6**. Summary diagrams of the chemical behavior of important radionuclide elements during normal operation of typical chloride or fluoride fueled MSRs (temperatures between 600 ºC -700 ºC). The chloride salt diagram (left) is adapted from Taube, 1978 and the fluoride salt diagram (right) is based from observations made during the MSRE (Compere et al., 1975).

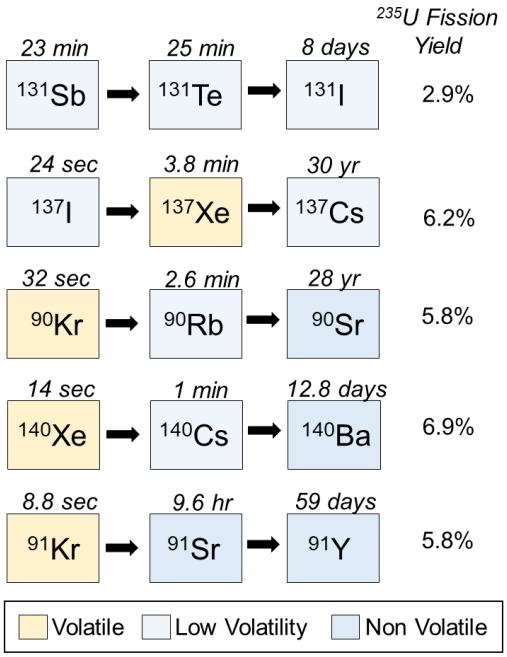


**Figure 7.** Portions of the decay chains of important fission product nuclides (fission yields are from Table 5 above).

There is less information regarding the disposition of fission products during operation of a chloride fuel salt-based reactor due to the lack of test reactor experience. However, the chemistry of fission products in molten chloride salts has been studied in some detail from both the perspective of MSR development (Taube, 1978) and their use in technologically mature pyroprocessing schemes (e.g., Steunenberg et al., 1969, Zhang, 2014). For example, Taube, 1978 suggests that I, Br, Se and Te would all be extracted during a gas purge through the fuel while the important fission products Ag, Pd, Rh, Ru and Tc would remain in the salt as nonvolatile metals. Molybdenum, Nb, Zr, Rb and Cs are identified as forming low volatility chloride species while the lanthanides, Sr and Ba are predicted to remain in the salt as nonvolatile chloride species (Taube, 1978).

The estimated fission product partitioning shown in Table 10 and Figure 8 is based on sample analyses from the MSRE (Compere et al., 1975) and assumptions made by (Robertson, 1971) about what elements will be held up within the chemical processing plant. The results show that many important fission products, including Se, Cd, Sn, Sb and the lanthanides, are predicted to remain entirely within the fuel salt, while the semi volatile elements (Cs, I), noble metals, and nuclides with noble gas precursors ($^{90}$Sr, $^{140}$Ba, $^{91}$Y) are predicted to be partitioned between the salt and the cover gas. A fraction of several important fission product elements is also predicted to adsorb or plate out onto metal surfaces or diffuse into the graphite moderator structures; these include Rb, Cs, Sr, Y, Zr, Te and the noble metals. It is assumed that a fraction of the Y, Zr, Nb, La, Pr, Nd, Pr and a large fraction of the Pa will be partitioned and held up within the fuel chemistry plant.

**Table 10**. Estimated distribution of important heat producing fission products for a normally operating fluoride-fueled MSR (quantified as thermal power). Adapted from Robertson, 1971.

| Element | At Reactor Shutdown | | | | 28 Hour Decay | | |
|---|---|---|---|---|---|---|---|
| | Salt | Off-Gas | Graphite/ Alloy | Chemistry Plant | Salt | Off-Gas | Graphite/ Alloy |
| | *kW* | *kW* | *kW* | *kW* | *kW* | *kW* | *kW* |
| **Zn** | 0.0002 | 0 | 0 | 0 | 0.00013 | 0 | 0 |
| **Ga** | 0.26 | 0 | 0 | 0 | 0.0047 | 0 | 0 |
| **Ge** | 1.8 | 0 | 0 | 0 | 0.083 | 0 | 0 |
| **As** | 45 | 0 | 0 | 0 | 0.14 | 0 | 0 |
| **Se** | 206 | 0 | 0 | 0 | 0.00023 | 0 | 0 |
| **Br** | 4220 | 0 | 0 | 0 | 0.014 | 0 | 0 |
| **Kr** | 1130 | 2370 | 250 | 0 | 0.016 | 2.8 | 0 |
| **Rb** | 5560 | 2930 | 290 | 0 | 0.0058 | 1 | 0 |
| **Sr** | 4270 | 374 | 40 | 1.5 | 131 | 220 | 23 |
| **Y** | 4750 | 140 | 17 | 170 | 267 | 79 | 7 |
| **Zr** | 648 | 0 | 0 | 350 | 349 | 0 | 0 |
| **Nb** | 314 | 1790 | 1790 | 318 | 406 | 97 | 97 |
| **Mo** | 69 | 835 | 835 | 0 | 0.024 | 145 | 145 |
| **Tc** | 25 | 1240 | 1240 | 0 | 0.003 | 30 | 30 |
| **Ru** | 2.5 | 160 | 160 | 0 | 0.002 | 88 | 88 |
| **Rh** | 4.1 | 52 | 52 | 0 | 0.0034 | 33 | 33 |
| **Pd** | 2 | 0.4 | 0.4 | 0 | 0.12 | 0.1 | 0.1 |
| **Ag** | 14 | 0.1 | 0.1 | 0.2 | 1.8 | 0 | 0 |
| **Cd** | 5.3 | 0 | 0 | 0 | 0.38 | 0 | 0 |
| **In** | 14 | 0 | 0 | 0 | 0.28 | 0 | 0 |
| **Sn** | 60 | 0 | 0 | 0 | 0.2 | 0 | 0 |
| **Sb** | 5450 | 0 | 0 | 0 | 14 | 0 | 0 |
| **Te** | 510 | 1970 | 1970 | 0 | 3.2 | 78 | 78 |
| **I** | 4510 | 2120 | 2120 | 0 | 48 | 745 | 745 |
| **Xe** | 1080 | 2770 | 414 | 0 | 28 | 180 | 22 |
| **Cs** | 4000 | 2600 | 383 | 0 | 2.5 | 8.1 | 0 |
| **Ba** | 4030 | 490 | 58 | 0 | 230 | 96 | 10 |
| **La** | 4620 | 470 | 50 | 68 | 1380 | 450 | 16 |
| **Ce** | 1260 | 3 | 0.5 | 154 | 375 | 3 | 0.5 |
| **Pr** | 1740 | 0 | 0 | 492 | 230 | 0 | 0 |
| **Nd** | 213 | 0 | 0 | 25 | 80 | 0 | 0 |
| **Pm** | 150 | 0 | 0 | 12 | 72 | 0 | 0 |
| **Sm** | 10 | 0 | 0 | 0.3 | 3.8 | 0 | 0 |
| **Eu** | 3.8 | 0 | 0 | 0.04 | 2.9 | 0 | 0 |
| **Gd** | 0.055 | 0 | 0 | 0 | 0.017 | 0 | 0 |
| **Tb** | 0.0024 | 0 | 0 | 0 | 0.0016 | 0 | 0 |
| **Pa** | 500 | 0 | 0 | 5000 | 485 | 0 | 0 |

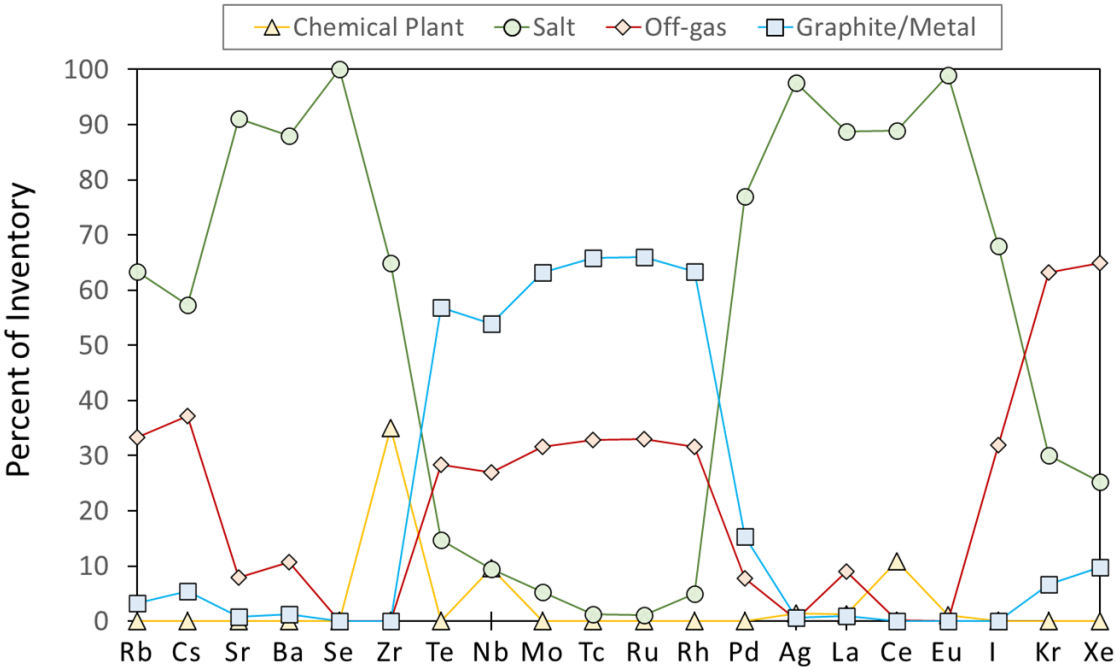


**Figure 8**. Distribution of important fission product elements for normal operation of a fluoride-fueled MSR. Values are based on those tabulated by Robertson, 1971.

# 4 Radionuclide Transport and Retention Phenomena

To conduct MST analyses, it is essential to have a comprehensive understanding of all potential radionuclide transport and retention mechanisms that control radionuclide release from a nuclear reactor. As stated in SECY-93-092, an MST is developed by modeling the transport of radionuclides from the fuel, through the reactor coolant system, through holdup volumes and barriers (including any mitigation features), and into the environment. In this section, general radionuclide transport and retention processes relevant to liquid fueled MSRs are discussed. These processes account for normal operating conditions and severe accidents, but their association with specific accident scenarios are not described in detail in this report.

A summary of the chemical and physical phenomena that control the transport and retention of radionuclides in a generic MSR is provided in Figure 9. The processes that can occur in the core vessel are the main focus of this section, but some transport phenomena may be important to other areas of an MSR design as well (e.g., off-gas system, fuel processing facility, and drain tank cell).

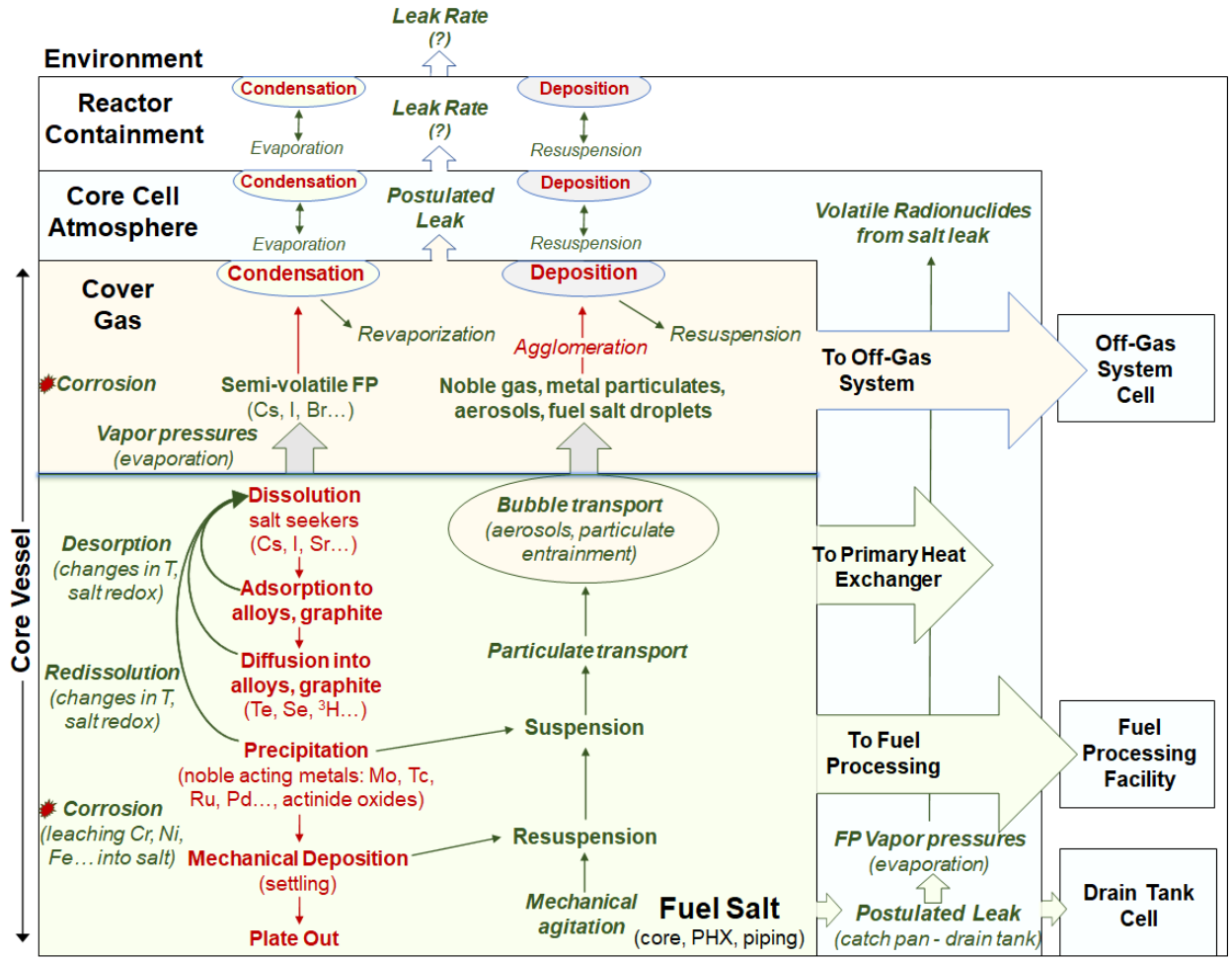


**Figure 9**. Schematic summary of radionuclide transport and retention phenomena pertaining to MSR core. Red text indicates retention processes; green text indicates transport processes.

### *4.1 Transport/Retention Processes Modeling with Thermochemical Data*

One of the foremost factors that determines whether a radionuclide will be retained or transported from the fuel salt is its chemical form, also referred to as chemical speciation. The chemical speciation of a radionuclide at any time point during normal operation or an accident scenario determines whether that radionuclide will partition into the vapor, liquid, or solid phase. If a radionuclide is released to the environment, its chemical speciation will affect transport and determine toxicity. The main factors that can influence chemical speciation in an MSR include total concentrations, fuel salt chemical composition, fuel salt redox potential, temperature, pressure, and reaction kinetics.

Grabaskas et al. (2016a) recently developed a model to calculate the speciation of key fission products for sodium fast reactor MST analyses using a thermochemical database and the modeling software HSC chemistry. Specifically, the chemical speciation and phase distribution was calculated at equilibrium by using the Gibbs free energy minimization method, which requires knowing the enthalpy and entropy of formation and the heat capacity for each possible species that may form. Activity coefficients must also be derived from experimental data and used as input in the software to account for the non-ideal behavior of

chemical species in the coolant-fuel mixture. A schematic that depicts how the thermochemical model calculates radionuclide speciation information used in the source term model is shown in Figure 10.

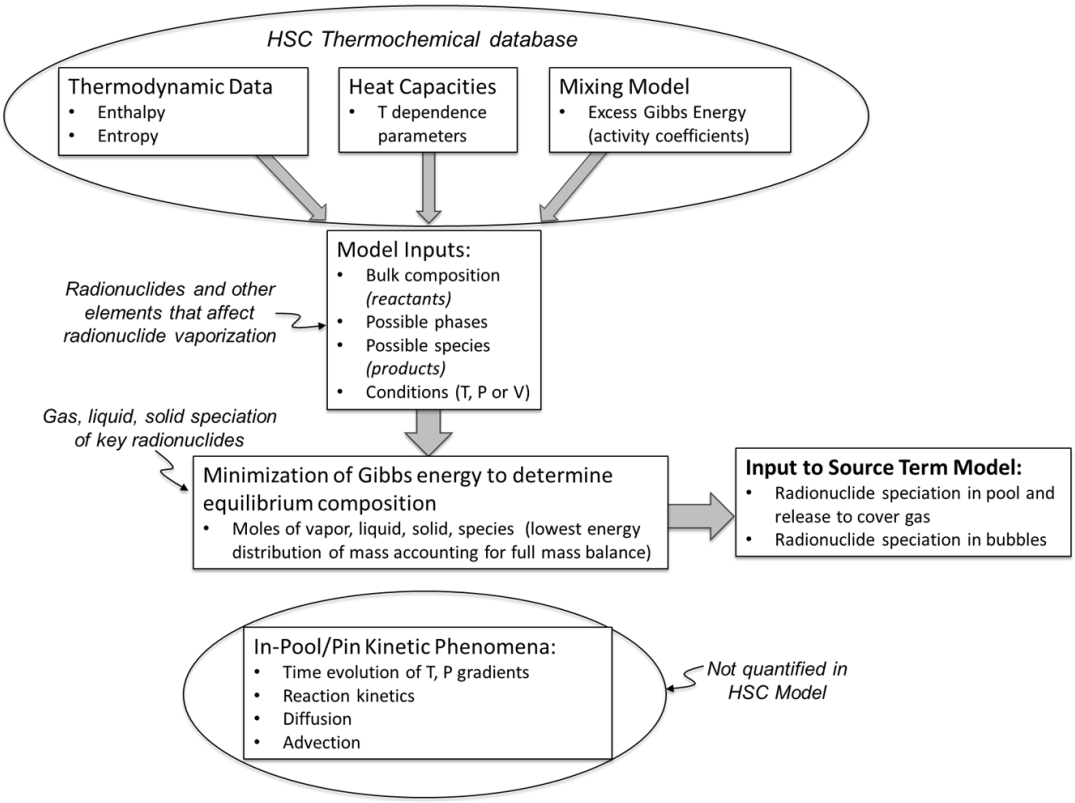


**Figure 10**. Schematic information flow for the thermochemical model used to calculate radionuclide chemical speciation for the sodium fast reactor MST (from Grabaskas et al., 2016a, Appendix C).

As shown in Figure 10, the methodology used previously for source term analysis of a sodium fast reactor did not consider reaction kinetics or physical processes that may create chemical gradients (e.g., advection and diffusion). The methodology is considered to be conservative because it assumes that chemical equilibrium was reached instantaneously.

### *4.2 Description of Transport and Retention Processes in a Generic MSR*

Chemically, liquid fueled MSR concepts can be grouped into two categories based on the halide used in the fuel salt: fluoride or chloride. Fluoride-based MSRs have been operated successfully and have received more historical attention than chloride-based fuel salts. Table 11 provides a non-comprehensive list of fuel salt compositions for MSR concepts to show the range of chemistries that are possible.

The fuel salt composition, relative abundance of chemical species, type of fissile material, and fuel salt oxidation state play an essential role on the possible transport and retention processes that may occur during normal operations or as a result of an accident. These transport and retention processes are discussed in detail below.

**Table 11.** MSR concept fuel salt chemistry (adapted from Taira et al., 2017).

| Concept | Feed | Molten Salt (mol %)[a] | Neutronic spectrum | Ref. |
|---|---|---|---|---|
| *Fluoride salts* | | | | |
| MSRE | $^{238}U$, $^{235}U$, $^{233}U$ | $LiF$-$BeF_2$-$ZrF_4$-$UF_4$ (65-29.1-5-0.9) | Thermal | Haubenreich and Engel, 1970; Grimes, 1970 |
| MSBR | $^{232}Th$, $^{233}U$ | $LiF$-$BeF_2$-$ThF_4$-$UF_4$ (71.6-16-12-0.4) | Thermal | Bettis and Robertson, 1970; Whatley et al., 1970 |
| MSFR | $^{232}Th$, $^{233}U$ | Fertile blanket $LiF$-$ThF_4$ (72-28) | Fast | Delpech et al., 2009; Merle-Lucotte et al., 2012; Mathieu et al., 2009 |
| MOSART | TRU 2-3 mol % | $LiF$-$NaF$-$BeF_2$ (15-58-27) | Fast | Ignatiev et al., 2007 |
| *Chloride salts* | | | | |
| WISE | Natural fuel $^{238}U$ or $^{232}Th$ | $Na^{37}Cl$-$An^{37}Cl_3$ (60-40) $Pb^{37}Cl_2$-$An^{37}Cl_3$ (60-40) | Hard fast | Slessarev and Bokov, 2003 |
| REBUS | TRU, U | (U, TRU)$Cl_3$-$NaCl$ TRU: 15.6 at. % | Fast | Mourogov and Bokov, 2006 |
| MCFBR | TRU, $^{238}U$ | Molten fuel: $PuCl_3$-$NaCl$ (15-85) Molten fertile material: $UCl_3$-$NaCl$ (65-35) | Fast | Taube and Ligou, 1972; Taube, 1978 |

[a] An = Actinide

### *4.2.1 Dissolution and Complexation*

Actinides are relatively soluble as fluoride and chloride complexes, but their solubility is heavily influenced by the redox potential of the fuel salt, temperature, and the presence of other metal fluoride or chloride complexes. Depending on fuel salt redox potential, uranium will exist as dissolved $UF_3$ and $UF_4$ complexes in fluoride fuel salts and $UCl_3$ and $UCl_4$ complexes in chloride salts. Fluoride fuel salts with uranium fuel typically use a mixture of $UF_4$ and $UF_3$ to act as redox buffers to prevent corrosion of structural metals by $UF_4$ (Toth et al., 1995). A $UF_4/UF_3$ ratio of 100 is estimated to provide enough $UF_3$ reductant to protect metal surfaces (Zhang et al., 2018). However, actinide trifluorides have limited solubility in fluoride salts. The solubility of $PuF_3$ in a range of fluoride fuel salt mixtures was 0.4 – 2.5 mol % at 650 °C and 0.16 – 1.0 mol % at 550 °C (Barton, 1960). Also, the presence of more than one actinide species can influence actinide solubilities. For example, the solubility of a $PuF_3$ and $UF_3$ mixture in a fluoride fuel salt is much less than individual solubilities of $PuF_3$ and $UF_3$ (Barton, 1960). Actinide trichlorides have a high solubility in chloride salts (relative to their fluoride counterparts), and thus, chloride fuel salts can contain significant amounts of actinides. The molten chloride fast breeder reactor concept has proposed a fuel salt composition of up to 40 mol % $PuCl_3$ in NaCl while still exhibiting a melt point below 500 °C (Taube, 1978). Actinide trichlorides are preferred over the more reactive actinide tetrachlorides (Flanagan et al., 2018). However, some actinide tetrachloride presence is favorable to minimize the disproportionation of actinide trichloride to actinide tetrachloride and actinide metal.

It is important to understand the solubilities and complexation behavior of the fission and activation products in an MSR salt. An analysis of the MSRE fuel salt determined that the majority of group IA (e.g., Rb, Cs), group IIA (e.g., Sr, Ba), lanthanide, Y, and Zr fission or activation products that were generated during operation are salt-soluble and remained homogenously distributed in the salt (Williams et al., 1996).

Although chemical speciation was not measured, it is inferred that these species formed stable fluoride complexes in the fuel salt.

Finally, the formation of fluoride or chloride compounds with fission products or metal alloy corrosion products in the fuel salt may decrease the solubility of actinides, especially polyvalent fluorides/chlorides. The presence of $CeF_3$ in a LiF-$BeF_2$ (63-37 mol %) salt mixture substantially decreases the solubility of $PuF_3$ (Barton, 1960). It is essential to monitor the salt chemistry to ensure actinides remain soluble throughout operation.

### *4.2.2 Volatilization*

The volatile species are the most likely to be released from reactor containment during normal operation or an accident scenario. The driving force for the volatilization of a chemical species from the molten fuel salt is the vapor pressure of the chemical species. Chemical species that can undergo volatilization in an MSR fall into three categories: the fuel salt compounds, the fission and activation products, and the actinides. One of the most appealing features of MSRs is the low vapor pressures of the fuel salt compounds, even at temperatures greater than 1000 °C (Table 12). Therefore, significant vaporization of salt compounds during a heating event is unlikely. For these reasons, MSRs are highly unlikely to experience over-pressurization events and differ significantly from LWRs in this respect.

**Table 12.** Measured vapor pressures of fuel salt compounds in simulated fuel salt

| *Measured vapor pressures over LiF-$ThF_4$-CsF (75.73-23.23-1.05 mol %)*[a] | | | |
|---|---|---|---|
| Temperature | 1100 K | 1200 K | 1300 K |
| $LiF_{(g)}$ | 0.5 Pa | 3.7 Pa | 19.4 Pa |
| $ThF_{4(g)}$ | 0.004 Pa | 0.09 Pa | 1.9 Pa |
| $CsF_{(g)}$ | 0.07 Pa | 0.3 Pa | 0.7 Pa |
| *Measured vapor pressures over pure FLiNaK (LiF-NaF-KF: 46.5-11.5-42.0 mol %)*[b] | | | |
| Temperature | 1000 K | 1100 K | — |
| $LiF_{(g)}$ | 0.1 Pa | 3.1 Pa | — |
| $NaF_{(g)}$ | -- | 0.4 Pa | — |
| $KF_{(g)}$ | 0.5 Pa | 10.3 Pa | — |

[a] From Capelli et al., 2018. [b] From Sekiguchi et al., 2019.

The volatile fission and activation products of interest that are expected to be released from fluoride or chloride fuel salts include noble gases (e.g., Xe and Kr), volatile halogen species (e.g., HF, $F_2$, $Cl_2$, $Br_2$, $I_2$, CsI), and volatile tritium species (e.g., $^3H_{2(g)}$, $^3HH_{(g)}$, and $^3HF_{(g)}$) (McFarlane et al., 2019). The noble gases will be released to the off-gas system during normal operation. If a leak occurs, noble gas fission products may build up in the head space of reactor containment or escape into the environment. Considering the large yield of noble gases through fission (nearly 1 atom per fission), pressurization of reactor containment spaces could occur and be an issue if an off-gas pathway is unavailable. Fission products Cs and I can bind together to form CsI, which is volatile in common MSR fuel salt compositions (i.e., FLiNaK and LiF-$ThF_4$-$UF_4$) (Kalilainen et al., 2020; Taira et al., 2017; Sekiguchi et al., 2019). In addition, CsI is considered one of the most important species transporting radioactive iodine under severe accident conditions for LWRs (Wright, 1994). Tritium will also be produced in MSRs due to ternary fission or activation of the fuel salt, coolant, and core materials, especially by the activation of $^6Li$ in the thermal neutron spectrum. Tritium is soluble in the fuel salt as $^3HF$ or $^3HCl$, but can undergo volatilization as $^3H_{2(g)}$, $^3HH_{(g)}$, or a halogen species (e.g., $^3HF_{(g)}$ or $^3HCl_{(g)}$) and readily diffuses through metal containment structures and the graphite moderator. Finally, non-volatile decay products generated from volatilized species may condense on containment surfaces (Compere et al., 1975). The $^{89}Sr$ and $^{137}Cs$ isotopes are decay products of the short-

lived noble gas species $^{89}Kr$ ($t_{1/2}$ = 3.18 min) and $^{137}Xe$ ($t_{1/2}$ = 3.83 min), respectively, and were detected outside of the fuel salt in the MSRE (Compere et al., 1975).

Compared to certain fission products, the actinide fluoride and chloride complexes have much lower vapor pressures. However, due to their high radiotoxicity and long half-lives, an MST requires detailed information on the vapor pressure of actinides as a function of fuel salt composition, total actinide concentration, and temperature. It is also important to note that $UCl_4$ is more volatile than other actinides anticipated to be present in MSR fuel salts (Flanagan et al., 2018).

Radiolysis is not expected to have a large influence on volatilization due to the high rate of recombination with the fuel salt expected at the temperatures of operation (Williams et al., 1996). However, volatile radiolysis products (e.g., $F_2$ and $Cl_2$) that do not recombine with the fuel salt (e.g., due to fuel salt cooling) may influence the redox potential of the fuel salt and production of volatile species. Evidence from the MSRE indicated that significant amounts of radiolytic $F_2$ were generated after reactor shutdown that recombined with the remaining $UF_4$ as the fuel salt cooled (Williams et al., 1996). The result was production of volatile $UF_{6(g)}$ and the subsequent deposition of 4.4 kg of uranium in the auxiliary charcoal bed of the off-gas system (Williams et al., 1996; Icenhour et al., 2001). Due to the high volatility and radiotoxicity of $UF_6$, opportunities for radiolytic $F_2$ and $UF_4$ to react should be monitored.

Table 13 outlines volatilization phenomena that may occur during normal operation or a postulated accident for a generic MSR. For each volatilization phenomenon described, Table 13 provides the source and the possible fate of the radionuclides of interest, the experimental or modeling evidence, potentially relevant accident scenarios, and any notes and references.

**Table 13**. Summary of volatilization phenomena.

| Description of phenomenon | Source of radionuclide species | Fate of radionuclide species | Experimental/ modeling details | Relevant accident scenarios | Notes | Ref. |
|---|---|---|---|---|---|---|
| Volatilization of medium-lived noble gas fission products (e.g., $^{85}Kr$) | Fission products of $^{233}U$, $^{235}U$, or $^{239}Pu$ in fuel salt | Release to cover gas and out-gas system | Evidence from MSRE operation | N/A [a] | none | [1] |
| Volatilization of short-lived noble gas fission products (e.g., $^{89}Kr$ and $Xe^{137}$) | Fission products of $^{233}U$, $^{235}U$, or $^{239}Pu$ in fuel salt | Release to cover gas and out-gas system | Evidence from MSRE operation | N/A [a] | none | [1] |
| | | Decay to non-volatiles daughters (e.g., $^{89}Sr$ and $^{137}Cs$) that may condense on containment surfaces | Evidence from MSRE operation | N/A [a] | none | [1] |
| Volatilization of CsI | Both fission products of $^{233}U$, $^{235}U$, or $^{239}Pu$ in fuel salt. $^{137}Cs$ is a decay daughter of $^{137}I$. $^{131}I$ is a | Release to cover gas and out-gas system. Environmental release via atmospheric | Vapor pressure modeling in LiF-$ThF_4$-$UF_4$ (78.8-16.9-4.2 mol %) fuel containing Cs and I | N/A [a] | Ref. [5] ran tests at 1 – 50 mol % CsI in FLiNaK at temp. = 823 – 1173 K. Csi vapor pressure varied with mol % CsI | [2] |

| | | | | | | |
|---|---|---|---|---|---|---|
| | decay daughter of $^{131}Sb$. | deposition. CsI is highly water soluble. | Vapor pressure measurements in LiF-NaF-KF (46.5-11.5-42 mol %) containing Cs and I | | Ref. [6] ran tests at 1 mol % CsI with and without 3.3 mol % CsF in FLiNaK at temp. = 900 – 1100 K. Cs and I had highest vapor pressures of any other element. | [3, 4] |
| Volatilization of KI | K = Salt component<br>I = Fission product of $^{233}U$, $^{235}U$, or $^{239}Pu$ | Release to cover gas and out-gas system. Environmental release via atmospheric deposition. KI is highly water soluble. | Vapor pressure measurements in FLiNaK | N/A [a] | Vapor pressure of KI under test conditions was unexpectedly high (e.g., $10^{-4}$ atm at 1000 K). | [3] |
| Volatilization of tritium as $^{3}HH$ or $^{3}H_2$ | Activation product of Li and/or Be in fuel salt or coolant salt (especially $^{6}Li$ in thermal neutron spectrum). Ternary fission product. $^{3}HH$ or $^{3}H_2$ can form from $^{3}H^{+}$ under reducing conditions. | Release to cover gas and out-gas system. Diffusion of tritium gas species through containment layers. | Evidence from MSRE | N/A [a] | $^{3}H^{+}$ can also corrode alloy surfaces, producing $^{3}HH$ or $^{3}H_2$. $^{3}HH$ may form depending on the presence of $^{1}H$ in reactor. | [5, 6] |
| Volatilization of $UF_6$ from cooled fuel salt | Reaction between $UF_4$ and $F_2$ or $F^0$ (produced from radiolysis) in cooled fuel salt. | Deposition in off-gas system | Evidence from MSRE | Fuel salt cooling | Measurements taken ~25 years after reactor shutdown and estimated loss of 4.4 kg of U from fuel salt as $UF_6$. Experimental evidence indicates annual reheating of cooled fuel salt to 200 °C to recombine $F_2$ with fuel likely led to inadvertent production of $UF_6$. | [7, 8] |
| Volatilization of $UCl_4$ at elevated temperatures | Formation of $UCl_4$ from $UCl_3$ under oxidizing conditions in chloride fuel salt | Deposition in off-gas system | Vapor pressure data | N/A [a] | $UCl_4$ has a boiling point of 791 °C | [9] |

[a] N/A indicates that the process is expected during normal operations but could also occur during an accident scenario
References: [1] Compere et al., 1975; [2] Kalilainen et al., 2020; [3] Taira et al., 2017; [4] Sekiguchi et al., 2019; [5] McFarlane et al., 2019; [6] Phillips and Easterly, 1980; [7] Williams et al., 1996; [8] Icenhour et al., 2001; [9] Flanagan et al., 2018

#### 4.2.2.1 Importance of Excess Gibbs Free Energy in Thermodynamic Modeling of Vapor Pressure for Mechanistic Source Term

Kalilainen et al. (2020) calculated the release of fission products and salt compounds from spilled LiF-$ThF_4$-$UF_4$ fuel salt in one of the first attempts to realistically model radionuclide release from an MSR under severe accident conditions. Specifically, evaporation from a salt surface that spilled on the floor of a confinement building was simulated by coupling the Gibbs Energy Minimization Software (GEMS), which employed the HERACLES thermodynamic database (Shcherbina et al.), with the severe accident code MELCOR.

The recommended approach to model MSR chemistry is the CALPHAD method, which enables the linkage of solution phase models to chemical and physical properties (McMurray et al., 2018). With this method, the Gibbs free energy of the solutions is described by Equation 1:

$$G = G^{ref} - T\Delta S + G^{EX} \quad (1)$$

where $G^{ref}$ is the weighted average of the Gibbs energies of each mixing constituent in a binary mixture (i.e., the "end members"), T is the temperature, and $\Delta S$ is the configurational entropy. The first two terms in the equation are related to ideal mixing and $G^{EX}$ is a parameter used to take non-ideal behavior due to mixing into account.

Kalilainen et al. (2020) noted the importance of including the excess Gibbs free energy for mixing of the salt components in the coupled thermodynamic and accident progression model. The excess Gibbs energy for different binary fluoride and iodide systems (see Table 14) was calculated empirically from published excess enthalpies and phase equilibria information (liquidus and solidus temperatures) and pure compound vapor pressures using the Redlich-Kister (Guggenheim) mixing model:

$$G_{ij}^{EX} = RTx_ix_j\left[a_0 + a_1(x_i - x_j) + a_2(x_i - x_j)^2 + \cdots\right] \quad (2)$$

where $a_0$, $a_1$, and $a_2$ are dimensionless fitting parameters and $x_i$ and $x_j$ are the mole fraction of species $i$ and $j$ in the binary system, respectively. The fitting parameters for the binary systems considered in that study are provided in Table 14.

**Table 14.** The Redlich-Kister mixing model fit parameters calculated for binary systems in the molten salt (from Kalilainen et al., 2020)

| Pair | $a_0$ | $a_1$ | $a_2$ |
|---|---|---|---|
| LiF–$ThF_4$ | –22105 | –22951 | –7122 |
| LiF–CsF | –16000 | 0 | 0 |
| CsI–LiI | –21478 | 4557 | –2607 |
| CsI–CsF | –2842.8 | 0 | 0 |
| LiF–LiI | –650 | 1036 | 338 |
| $ThF_4$–$ThI_4$ | –62000 | 0 | 0 |
| LiI–$ThI_4$ | –22105 | –22951 | –7122 |
| LiF-$UF_4$ | –30046 | –31196 | –9681 |
| CsF–$ThF_4$ | –145000 | 0 | 0 |
| CsI–$ThI_4$ | –19575 | 5763 | 4090 |

The modeled evaporation behavior of $UF_{4(g)}$ and $CsI_{(g)}$ is markedly different when the effects of salt mixing are considered than when just the pure compound vapor pressures are used (Figure 11). The model that included salt mixing showed an overall reduced fission product release and delayed release due to the effect of mixing on evaporation temperatures in comparison to pure compound simulations.

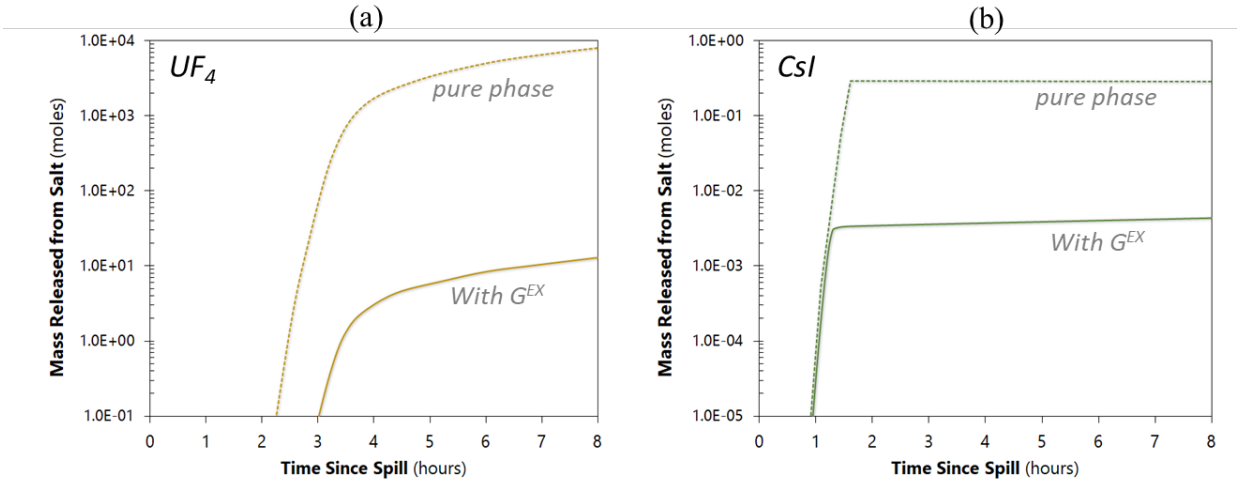


**Figure 11**. Analysis of a) $UF_4$ and b) CsI volatilization after spill of LiF-$ThF_4$-$UF_4$ fuel salt containing Cs and I that emphasizes the importance of experimentally quantifying non-ideality (adapted from Kalilainen et al., 2020).

### *4.2.3 Precipitation*

The precipitation of chemical species in the MSR fuel salt can lead to particulates circulating within the primary coolant, particulate settling and potential blockage of flow, and plate-out and increased decay heat in certain locations. In addition, the precipitation of fissile material could violate the reactivity control fundamental safety function (FSF). Actinides and noble metals are the predominant chemical species likely to precipitate in the MSR fuel salt. In the MSRE, noble metals (e.g., Nb, Mo, Tc, Ru, Rh, Pd, Ag, Sb, and Te) dissolved in the fuel salt to a minor extent but mainly deposited on surfaces (Compere et al., 1975).

As stated in Section 4.2.1, actinide fluoride and chloride complexes are soluble in fluoride and chloride fuel salts, respectively. However, their solubility limits depend on the fuel salt redox potential, temperature, the presence of competing metals (e.g., lanthanides), and the presence of water or oxygen. The onset of reducing conditions in the fuel salt due to the loss of radiolytic $F_2$ or $Cl_2$ or the introduction of a reductant (e.g., liquid metal coolant during an accident scenario) could cause fuel salt components and actinides to precipitate out as metals. Table 15 shows the reduction potentials of major fuel salt constituents in LiF-$BeF_2$ (67-33 mol %). At the onset of reducing conditions in the fuel salt, the metal species will precipitate in their metallic form according to their redox potentials: Li > Be > U ~ Zr (Compere et al., 1975).

**Table 15.** Reduction potentials of major fuel salt constituents (adapted from Williams, D. F. et al., 1995).

| | E° = reduction potential (V) [a] | |
|---|---|---|
| Half-cell reaction | 450 °C | 725 °C |
| $Li^{+} + e^{-} \longrightarrow Li_{(s)}$ | -2.770 | -2.559 |
| $Be^{2+} + 2e^{-} \longrightarrow Be_{(s)}$ | -1.958 | -2.460 |
| $U^{3+} + 3e^{-} \longrightarrow U_{(s)}$ | -1.606 | -1.433 |
| $U^{4+} + 4e^{-} \longrightarrow U_{(s)}$ | -1.522 | -1.336 |
| $Zr^{4+} + 4e^{-} \longrightarrow Zr_{(s)}$ | -1.542 | -1.335 |
| $U^{4+} + 4e^{-} \longrightarrow U^{3+}$ | -1.268 | -1.045 |

[a] Potentials referenced to $HF/H_2$, $F^-$ in $0.67LiF\text{-}0.33BeF_2$

Williams et al. (1995) stated that the development of highly reducing conditions was one of the chief concerns of the original MSRE researchers due to the "likelihood of catastrophic phase segregation" through the precipitation or plate-out of fuel salt components in their metallic form. Thus, the redox chemistry of the fuel salt was diligently monitored to ensure highly reducing conditions did not develop.

In fluoride fuel salts, $UF_3$ abundance relative to $UF_4$ must be maintained to prevent the reaction of $UF_3$ with moderator graphite to produce insoluble uranium carbides (Zhang et al., 2018; Toth et al., 1995) or the disproportionation of $UF_3$ into $UF_4$ and $U^0$ (Grimes, 1964). Similarly, $UCl_3$ may disproportionate into $UCl_4$ and $U^0$ in chloride salts (Taube and Ligou, 1972). Actinides or salt soluble fission or corrosion products (e.g., Zr, Ti, Al, Fe, Cr, Mn, or Mg) can react with $O_2$ or $H_2O$ in the fuel salt or other reactor systems (e.g., fuel processing) to form insoluble metal oxides, which may disrupt the fuel system (Taube and Ligou, 1972). Lanthanide fission products may also compete with actinides in the formation of soluble fluoride or chloride complexes in the salt, which could limit actinide solubility. For example, the presence of $CeF_3$ at a 1:1 and 5:1 molar ratio to $PuF_3$ dramatically decreased $PuF_3$ solubility in a $LiF\text{-}BeF_2$ (63-37 mol %) fuel salt. It is therefore necessary to have a detailed understanding of the solubility of actinide fluoride and chloride complexes in a range of fuel salt compositions (including the effect of fission product presence) and temperatures.

Table 16 outlines precipitation phenomena that may occur during normal operation or a postulated accident for a generic MSR. For each precipitation phenomenon, Table 16 provides the source and the possible fate of the radionuclides of interest, the experimental or modeling evidence, potentially relevant accident scenarios, and any notes and references.

**Table 16.** Summary of precipitation phenomena.

| Description of phenomenon | Source of radionuclide species | Fate of radionuclide species | Experimental/ modeling details | Relevant accident scenarios | Notes | Ref. |
|---|---|---|---|---|---|---|
| Deposition (plate out) of noble metals onto metal or graphite surfaces in fuel salt | Fission products of $^{233}U$, $^{235}U$, or $^{239}Pu$ in fuel salt | Retention in fuel salt. Build up on containment surfaces and graphite moderator. | Evidence from MSRE | N/A [a] | Plate out of highly radioactive noble metals can cause increased heat deposition in certain locations and result in localized shielding requirements. | [1, 2] |
| Precipitation of uranium metal in fuel salt under reducing conditions | $UF_4/UF_3$ or $UCl_4/UCl_3$ in fuel salt. Reduction caused by introduction of reductant to fuel salt. | Settling of uranium metal in fuel salt. Uncontrolled criticality. | Evidence for creation of reducing conditions due to radiolytic $F_2$ generation from MSRE. | Normal operations. Inadvertent introduction of liquid metal coolant (i.e., NaK) to fuel salt. Fuel salt cooling. | Radiolytic generation and escape of $F_2$ from fuel salt can create reducing conditions that favor $U(IV)F_4$ reduction to U(0) metal. Inability of radiolytic $F_2$ to recombine with fuel salt due to fuel salt cooling can promote this phenomenon. | [3] |
| Precipitation of uranium metal via disproportion-ation reactions | Disproportion-ation of $UF_3$ in fluoride salt or $UCl_3$ in chloride salt | Settling of uranium metal in fuel salt. Uncontrolled criticality. | Chemical tests for MSRE development. | Too much $UF_3$ in fuel salt relative to $UF_4$. | $4UF_3 = 3UF_4 + U^0$<br>$4UCl_3 = 3UCl_4 + U^0$ | [4, 5] |
| Precipitation of uranium carbides ($UC_x$) | Reaction between $UF_3$ and graphite moderator (C) | Settling in fuel salt. Uncontrolled criticality. | Evidence from MSRE | N/A [a] | $4UF_3 + xC = 3UF_4 + UC_{x(s)}$ | [3, 6] |
| Precipitation of actinide metal oxides | Actinides in fuel salt or fertile coolant material. | Settling in fuel salt. Uncontrolled criticality. | Evidence from fluoride and chloride salt experiments. | Exposure of fuel to moisture ($H_2O$) or $O_2$ | $2H_2O_{(g)} + UF_4 = UO_{2(s)} + 4HF_{(g)}$ | [4, 6] |
| Precipitation of fission product metal (Me) as oxides | Salt soluble metal fission products. | Settling in fuel salt. Disruption of fuel salt flow. | Evidence from chloride salt experiments. | Exposure of fuel to moisture ($H_2O$) or $O_2$ | $MeCl_2 + H_2O = MeO + 2HCl$<br>$MeCl_2 + O_2 = MeO + Cl_2$ | [4] |
| Precipitation of actinide trifluorides in presence of lanthanide trifluorides | Fuel salt actinides. | Settling in fuel salt. Uncontrolled criticality. | $PuF_3$ solubility tests in LiF-$BeF_2$ (63-37 mol %) with competing fluorides. | N/A [a] | The presence of $CeF_3$ at a 1:1 and 5:1 molar ratio to $PuF_3$ dramatically decreased $PuF_3$ solubility.<br>The presence of $BaF_2$ and $ThF_4$ also decreased solubility of $PuF_3$. | [7] |

[a] N/A indicates that the process is expected during normal operations and could occur during an accident scenario.
References: [1] Compere et al., 1975; [2] Flanagan et al., 2018; [3] Zhang et al., 2018; [4] Taube and Ligou, 1972; [5] Grimes, 1964; [6] Toth et al., 1995; [7] Barton, 1960.

### *4.2.4 Physical transport and retention phenomena*

Physical phenomena including bubble bursting, spraying, misting, and aerosol transport can be a source of radionuclide migration into the cover gas region and lead to the deposition of radionuclides on containment surfaces. During the operation of the MSRE, fuel salt droplets were released from the salt surface and

deposited onto a stainless-steel metal strip in the pump bowl gas space during just a 10-hour exposure period (Figure 12). The salt droplets formed from mist produced at the fuel surface, which is evident from the higher salt droplet density at the end of the strip nearest to the fuel salt (the left side of Figure 12).

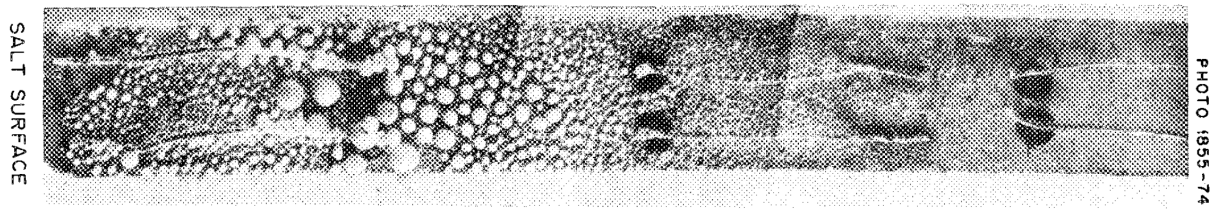


**Figure 12.** Salt droplets on a stainless-steel metal strip that formed due to exposure to the pump bowl gas space of the MSRE for 10 hours (from Compere et al., 1975).

Thermodynamic modeling will not represent the physical transport processes described above and other modeling tools will be needed to fully account for the transport of radionuclides. As part of MST analyses for the sodium fast reactor, for example, the bubble transport processes were quantified with the IFR bubble code developed at Argonne (Grabaskas et al., 2016a). Although bubble formation mechanisms will be different in MSRs, bubbles are expected to be a pathway to transport entrained radionuclides during normal operations or an accident scenario.

Another important physical process pertinent to modeling accident scenarios is liquid immiscibility (e.g., fuel salt and coolant salts). For example, a fast spectrum reactor may utilize liquid lead as a reflector blanket, which has low miscibility with chloride salts.

# 5 Source Term Model for Salt Spill Bounding Accident

The early developmental work on MSRs in the 1960s – 1970s including the MSRE, MSBR, MSDR and the denatured molten salt reactor development (DMSR) projects all concluded that a breach in the primary system leading to a spill of fuel salt into containment represents the maximum credible accident for MSR designs (e.g., Rosenthal et al., 1972, Engel et al., 1979). On-going developmental work on modern MSR concepts also identifies a fuel salt spill from a rupture in the primary system as the primary bounding accident (e.g., Yoshioka and Kinoshita). As perhaps the first attempt to mechanistically model the release of key fission products and actinides during a salt spill accident, the work of Kalilainen et al., 2020 provides a useful guide for future MSR mechanistic source term development projects and is discussed in detail as a case study for guiding future MST development.

## *5.1 Salt Spill Simulation Design and Methodology*

The MSR reference design used in the Kalilainen et al. MST study was the European Commission-funded molten salt fast reactor (MSFR) project. The MSFR is a fast neutron spectrum reactor with a nominal fuel salt composition of LiF-$ThF_4$-$UF_4$ (77.5-20-2.5 mol %). A simplified diagram of the major components of the MSFR design is shown in Figure 13.

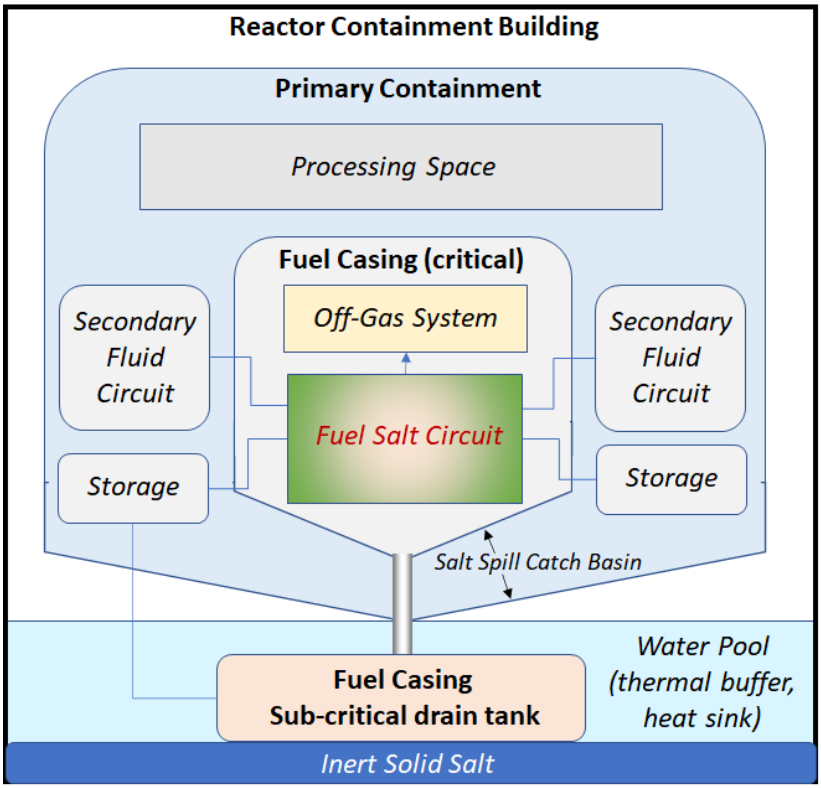


**Figure 13**. Schematic diagram showing the major components of the MSFR primary fuel salt loop (adapted from Kloosterman, 2017).

The accident scenario modeled by Kalilainen et al. involved a postulated rupture of the fuel salt circuit and primary fuel casing leading to fuel salt draining onto the catch basin within the primary containment (i.e., the "floor") shown in Figure 13. The containment atmosphere is assumed to be pure nitrogen. The purpose of the study was to model the temperature evolution of the spilled salt, the evaporation behavior of the salt and the release of Cs and I species during evaporation. The radionuclide inventory of the fuel salt was determined using EQL0D (Hombourger et. al., 2020) and the temperature evolution and fission product release processes were modeled using MELCOR 2.2 coupled with the thermodynamic Gibbs energy minimization code GEMS (Kalilainen et al., 2020). The evaporation processes and thermal-hydraulic conditions in containment were modeled using MELCOR, while salt and fission product speciation and vapor pressures were determined using GEMS. The GEMS code accounted for the non-ideality of the fuel salt chemistry using the methods discussed in Section 4.2.2. All of the species considered in the Kalilainen et al. salt spill simulation are listed in Table 17.

**Table 17**. Chemical species included in the MELCOR – GEMS model of the MSFR salt spill accident (adapted from Kalilainen et al., 2020).

| Solids | Liquids | Gases |
|---|---|---|
| $Li_7ThUF$ | CsF(l) | Cs(g) |
| $LiThU_4F_{17}$ | CsI(l) | $Cs_2$(g) |
| Cs | LiF(l) | $Cs_2F_2$(g) |
| CsF | $ThF_4$(l) | CsF(g) |
| CsI | $ThI_4$(l) | $Cs_2I_2$(g) |
| $Cs_2Th_3F_{14}$ | $UF_3$(l) | CsI(g) |
| $Cs_2ThF_6$ | $UF_4$(l) | CsLi(g) |
| $Cs_3ThF_7$ | — | F(g) |
| $CsTh_2F_9$ | — | $F_2$(g) |
| $CsTh_3F_{13}$ | — | I(g) |
| $CsTh_6F_{25}$ | — | $I_2$(g) |
| a-$CsThF_5$ | — | Li(g) |
| $Cs_2ThI_6$ | — | $Li_2F_2$(g) |
| $I_2$ | — | $Li_3F_3$(g) |
| Li | — | LiF(g) |
| $LiCsF_2$ | — | $Li_2I_2$(g) |
| LiF | — | $Li_3I_3$(g) |
| LiI | — | LiI(g) |
| $Li_2O$ | — | Th(g) |
| $Li_3ThI_7$ | — | $ThF_2$(g) |
| $Li7Th_6F_{31}$ | — | $ThF_3$(g) |
| $LiTh_4F_{17}$ | — | $ThF_4$(g) |
| $Li_3ThI_7$ | — | ThI(g) |
| $LiTh_2I_9$ | — | $ThI_2$(g) |
| $LiTh_4I_{17}$ | — | $ThI_3$(g) |
| $LiThI_5$ | — | $ThI_4$(g) |
| $Li_4UF_8$ | — | U(g) |
| $Li_7U_6F_{31}$ | — | UF(g) |
| $LiU_4F_{17}$ | — | $UF_2$(g) |
| Th | — | $UF_3$(g) |
| $ThF_4$ | — | $UF_4$(g) |
| ThI | — | UI(g) |
| $ThI_2$ | — | $UI_2$(g) |
| $ThI_3$ | — | $UI_3$(g) |
| $ThI_4$ | — | $UI_4$(g) |
| U | — | — |
| $U_2F_9$ | — | — |
| $U_4F_{17}$ | — | — |
| $UF_3$ | — | — |
| $UF_4$ | — | — |
| $UI_3$ | — | — |
| $UI_4$ | — | — |

Calculations to determine the composition of the fuel salt assume that the MSFR fuel is reprocessed using a batch-wise extraction and processing rate of 40 liters per day. For this process, volatile fission products were continuously removed while soluble fission products were not removed. The fission product composition of the fuel salt assumed 200 equivalent full power years of operation (Kalilainen et al., 2020). A simplified schematic of the MSFR fuel cycle and the context of the salt spill accident assumed by Kalilainen et al. is shown in Figure 14. The concentration of iodine in the fuel salt is relatively low because the iodine precursor isotopes of Sb and Te are largely removed by the off-gas system with a cycle time of 43 seconds (Kalilainen et al., 2020). Similarly, the Cs concentration in the fuel salt is also relatively low because its precursor isotopes of Te and Xe are largely removed by the off-gas system. Note that the rate and efficiency at which metals such as Sb and Te will be partitioned to the off-gas is strongly dependent on the sweep gas system design and the redox conditions of the salt (Kalilainen et al., 2020). However, it was assumed that the cycle time for the removal of metallic fission products (e.g., Sb and Te) is the same as the

noble gases (43 seconds) (Kalilainen et al., 2020). The initial composition of the fuel salt based on these assumptions is given in Table 18.

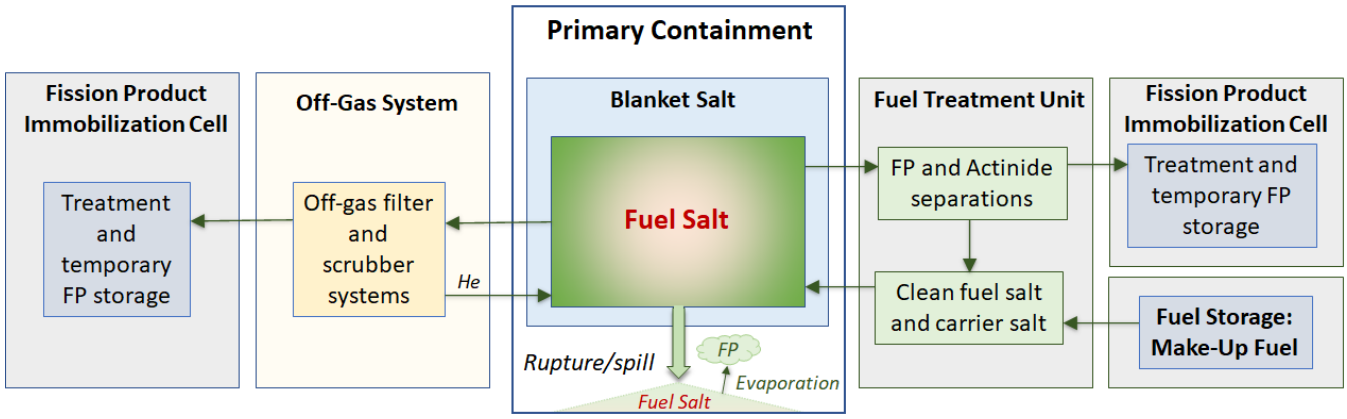


**Figure 14**. Simplified fuel cycle flow diagram for the MSFR showing the context of a fuel salt spill accident (adapted from Kalilainen et al., 2020).

**Table 18**. Initial composition of fuel salt used in salt spill simulation (adapted from Kalilainen et al., 2020).

| Initial composition of fuel salt | (mol %) | Initial masses in initial fuel salt | (kg) |
|---|---|---|---|
| LiF | 78.8 | Li | 4720.0 |
| ThF4 | 16.9 | Th | 33910.0 |
| UF4 | 4.2 | U | 8650.0 |
| Cs | 9.8x10-3 | Cs | 11.0 |
| I | 5.8x10-5 | I | 0.06 |
| | | F | 26787.0 |

The MSFR containment geometry and decay heat removal assumed for this study was a simplified design based on Wang et al., 2019. The confinement volume, geometry, initial conditions and boundary conditions can all have significant effects on source term modeling results. However, since the Kalilainen et al. study focused specifically on developing fission product release models that account for non-ideality of the fuel salt chemistry, a relatively simple primary containment system was assumed (Kalilainen et al., 2020).

The containment geometry used to define the salt spill simulation in MELCOR is shown in Figure 15. The containment room was modeled as a cylindrical container divided into 14 control volumes with a salt layer on the floor. This containment volume was assumed to contain the fuel casing from which the fuel salt has drained and a gas-gas heat exchanger that encircles the containment room at a distance of 15 m above the spilled fuel salt surface. The initial confinement atmosphere was assumed to be 100% nitrogen at 1 bar pressure (Kalilainen et al., 2020). The control volume layout is used to model convective heat transfer and the transport of evaporated species within the containment volume. All surfaces were assumed to be adiabatic except for the heat exchanger and salt surface. A natural convective gas flow within containment is driven by the thermal gradient between the hot salt surface and the colder heat exchanger. Heat conduction and thermal radiation were taken into account in the MELCOR simulation (Kalilainen et al., 2020). The radiation emissivity of the MSFR salt is unknown so the value of 0.44 measured for sodium sulfate was used (Kalilainen et al., 2020).

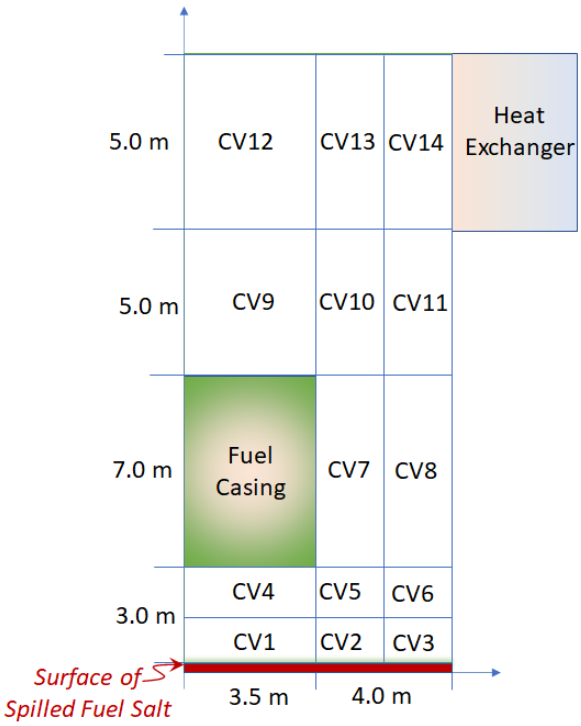


**Figure 15**. Containment geometry and control volume (CV) layout used in MELCOR to simulate fuel salt evaporation and fission product release (adapted from Kalilainen et al., 2020).

Time zero for the salt spill simulations was assumed to be at the moment the fuel salt spilled onto the containment floor and the salt was assumed to form a uniform layer. The initial heating rate of the salt due to decay heat is 6 ºC per minute and the initial salt temperature was assumed to be 27 ºC. This low initial salt temperature was used so the salt component and fission product speciation could be studied over a broad temperature range (Kalilainen et al., 2020). The temperature evolution of the salt and containment atmosphere (control volume CV13 in Figure 15) calculated by the MELCOR model are shown in Figure **16**a. The results show the spilled fuel salt reaches a maximum temperature of 1225 ºC approximately 3 hours after the spill occurs in this containment geometry (Kalilainen et al., 2020). Figure 16b shows the pressure generated in containment due to the fuel salt heat up calculated by the coupled MELCOR-GEMS model.

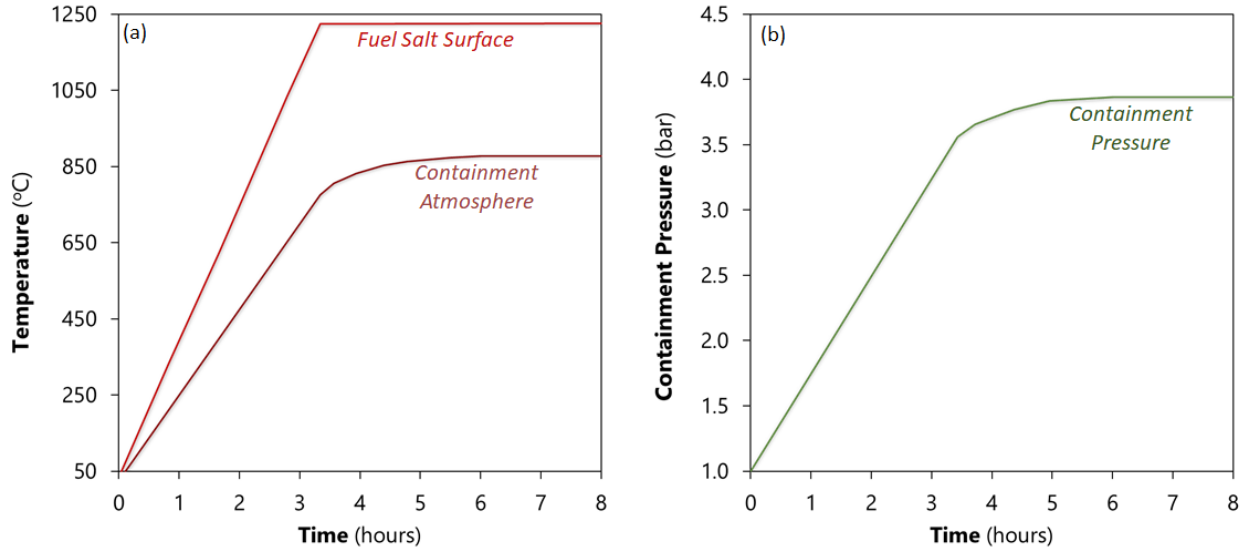


**Figure 16.** Temperature and pressure evolution of fuel salt and containment atmosphere following the salt spill (adapted from Kalilainen et al., 2020).

To simulate the evaporation of species from the salt surface, the following relationship was defined and embedded in MELCOR:

$$\frac{dm_i}{dt} = Ak_i(C_i^s - C_i^a) \tag{3}$$

This gives the evaporation rate of a species $i$ from the salt surface to the neighboring control volume, where $m$ is mass, $A$ is the area of the salt surface (i.e., the surface area of the containment where the evaporation is taking place), $k_i$ is the mass transfer coefficient, $C_i^s$ is the saturation concentration of species $i$ (based on the saturation vapor pressure of the species $P_i^s$) and $C_i^a$ is the concentration of species $i$ in the control volume atmosphere directly above the spilled salt. This model assumes the salt and the gas atmosphere near the salt have equilibrated (Kalilainen et al., 2020). Evaporation of $i$ from the salt surface will occur at a rate defined by Equation 3 as long as the concentration in the control volume atmosphere remains unsaturated. This calculation assumes direct proportionality between the mass transfer coefficient $k_i$ and the diffusivity of species $i$ based on "film theory" used in simplified mass transfer calculations (Kalilainen et al., 2020).

The saturation vapor pressure $C_i^s$ in Equation 3 is incorporated into MELCOR as a function of temperature as described by:

$$log_{10}P_i^s = A + \frac{B}{T} + C \cdot log_{10}T \tag{4}$$

where the coefficients $A, B, C$ are obtained by using GEMS or from literature values (Kalilainen et al., 2020). For these models, MELCOR tracks the elemental composition of the salt throughout the evaporation simulation, whereas the GEMS code uses these compositions to determine the salt speciation at every time step (Kalilainen et al., 2020).

Kalilainen et al. used the following steps to model the salt spill scenario summarized in Figure 15 and the related text above:

1. Ran accident simulation in MELCOR for 200 seconds.

2. Collected salt composition and temperature results from MELCOR time step and passed to GEMS for the speciation calculations.
3. Ran GEMS code for the first 200 second step.
4. Collected species concentrations and vapor pressure results from GEMS and passed to MELCOR using a new input file.
5. Repeated steps 1 – 4 for the duration of the simulation.

The vapor pressure information for different species was passed to MELCOR in the form of the coefficients $A, B, C$ (see Equation 4). The binary interaction parameters used in GEMS to account for the non-ideal solution behavior were identified in Table 14.

### *5.2 Summary of Salt Simulation Results*

As discussed in Section 4.2.2, Gibbs free energy minimization calculations that ignore the excess Gibbs energy functions (usually quantified as activity coefficients) can lead to inaccurate predictions of the chemical behavior of a molten salt. The non-ideal solution behavior (quantified by excess Gibbs energy) of molten salts manifests in several ways that can influence the salt behavior during both normal and accident conditions. The effects include:

- an increase or decrease in melting temperatures relative to those predicted assuming ideal behavior,
- the occurrence of miscibility regions not predicted by ideal behavior models and,
- significant deviations in species vapor pressures relative to those predicted by ideal models.

For molten salts, the excess Gibbs energies are generally negative, which causes a decrease of the melting temperatures relative to ideal behavior and a relative decrease in vapor pressures of the molten salt components. Kalilainen et al. quantified the effects of non-ideal behavior by performing some simulations in which the excess Gibbs energy was accounted for (Case 1, the best estimate modeling case) and other simulations in which the default MELCOR pure compound species vapor pressures were used (Case 2). The pure phase vapor pressures do not account for non-ideality and generally over-predict species vapor pressures. This can be seen in Figure 17, which shows some example simulation results. Other example results highlighting the dramatic difference between Case 1 (which accounts for mixing) and Case 2 (which does not account for mixing) are shown in Figure 18.

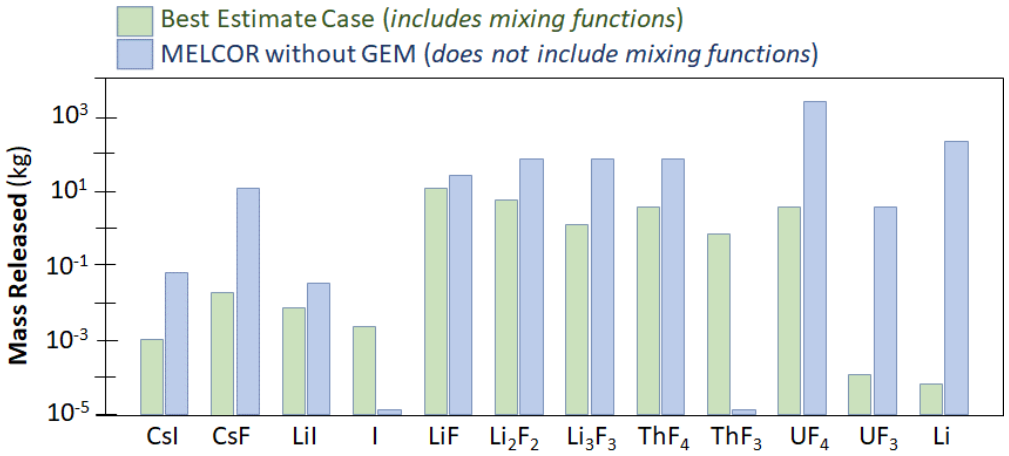


**Figure 17**. Example results comparing simulations that account for non-ideality (green) and those using pure phase vapor pressures (blue) (adapted from Kalilainen et al., 2020). Both sets of results are for the end of the simulation where the salt temperature has reached approximately 1225 ºC (see Figure 4).

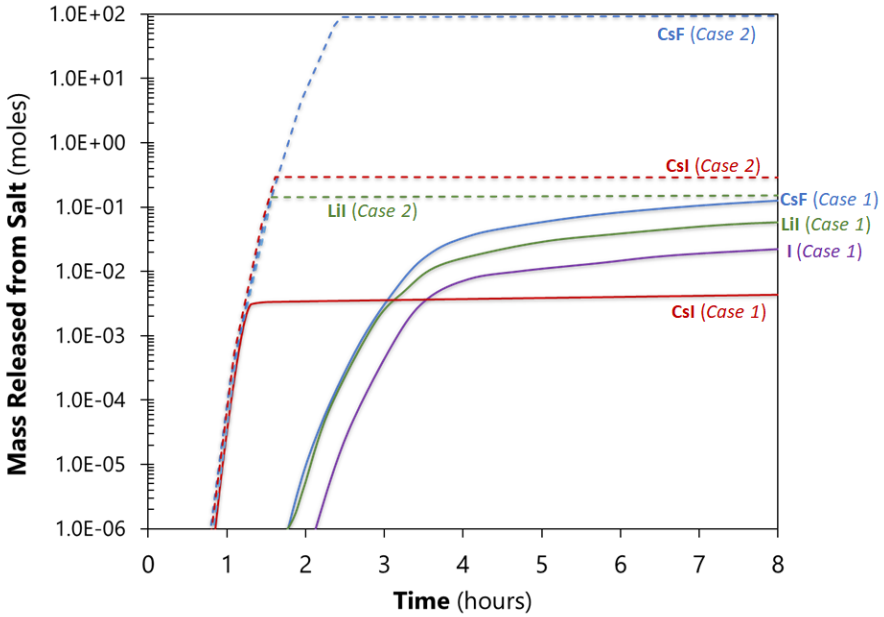


**Figure 18**. Vapor species released form evaporating salt for the Kalilainen et al. Case 1 (non-ideal behavior) and Case 2 (ideal behavior) simulations (adapted from Kalilainen et al., 2020).

The Kalilainen et al. salt spill simulation study found that the thermal-hydraulic variables and parameters having the strongest effect on the fuel salt evaporation and fission product vaporization behavior were the salt and containment atmosphere temperatures, the containment pressure and the mass transfer coefficient at the salt surface ($k_i$ in Equation 3). The temperature shows little to no stratified layers within the containment atmosphere (Kalilainen et al., 2020). This is due to significant mixing by natural convection induced by the temperature difference between the spilled salt and the heat exchanger (see Figure 15 for layout).

As shown in Figure 17, the evaporated masses of Li, $UF_3$ and $UF_4$ calculated using the coupled MELCOR-GEMS model that accounts for the non-ideal mixing (Case 1) are considerably lower than those calculated using the MELCOR model with pure phase vapor pressures (Case 2). This is due to the species interactions that are quantified by Equation 2. The species $ThF_4$, $Li_3F_3$, $Li_2F_2$ and LiF also all show lower mass release rates for Case 1 relative to Case 2. Note that the species I and $ThF_3$ were not considered in the pure phase evaporation calculations (Case 2) (Kalilainen et al., 2020).

The released masses of CsI, CsF, I and LiI are shown in Figure 18. It is noted that CsI starts to evaporate from the fuel salt at about the same time in both Cases 1 and 2. This is due to the relatively high vapor pressure of CsI and the fact that it is present as a separate solid phase at simulation times less than 1 hour (Kalilainen et al., 2020). At simulation times greater than 2 hours, the temperature of the salt exceeds the melting point of CsI (~620 °C) and so its components begin to interact with other species in the Li-Th-F melt. This results in a lower vapor pressure of CsI for Case 1 relative to Case 2 (Figure 18).

For Case 2, CsI, CsF and LiI all begin to evaporate nearly simultaneously because of their similar pure phase vapor pressures (Kalilainen et al., 2020). Also for Case 2, CsI and LiI release stops when the iodine is depleted from the salt (indicated by constant mass in Figure 18), whereas CsF release continues until Cs is depleted. Due to the slower releases of the cesium and iodine species in Case 1, the release curves show more gradual shifts to lower release rates (Figure 18) (Kalilainen et al., 2020). The species CsF shows a delayed evaporation in Case 1 relative to Case 2 due to its retention in the salt solutions at temperatures below the melting point of the mixture. This is due the formation of intermediate Cs-Th-F compounds such as $CsTh_3F_{13}$ (Kalilainen et al., 2020).

# 6 Engineering-Scale Tests

## *6.1 Salt Spill Validation Tests*

The bounding accident (maximum credible accident) used in the safety evaluation of the MSRE involved a dual failure event in which piping containing the fuel salt failed leading to hot salt spilling onto the containment floor followed by rupture in a water line that was part of a cooling system. The reaction of the cooling water with the hot salt was postulated to cause a pressure spike, containment rupture (through a rupture disk), and the subsequent pressure-driven transport of radionuclides that were released from the fuel salt (Beall et al., 1964). This type of event would be precluded in newer MSR designs that avoid the use of systems containing enough water to pressurize containment within the primary loop. The possibility of a rupture within the primary loop leading to hot fuel salt spilling onto the containment floor cannot be precluded and is deemed to be the primary event within an MSR bounding accident. There remain significant uncertainties as to the thermal and chemical consequences of such a salt spill event. The salt spill test discussed below provides fundamental data needed to reduce these uncertainties and facilitate the development and validation of thermal-hydraulic and source term models for such an event.

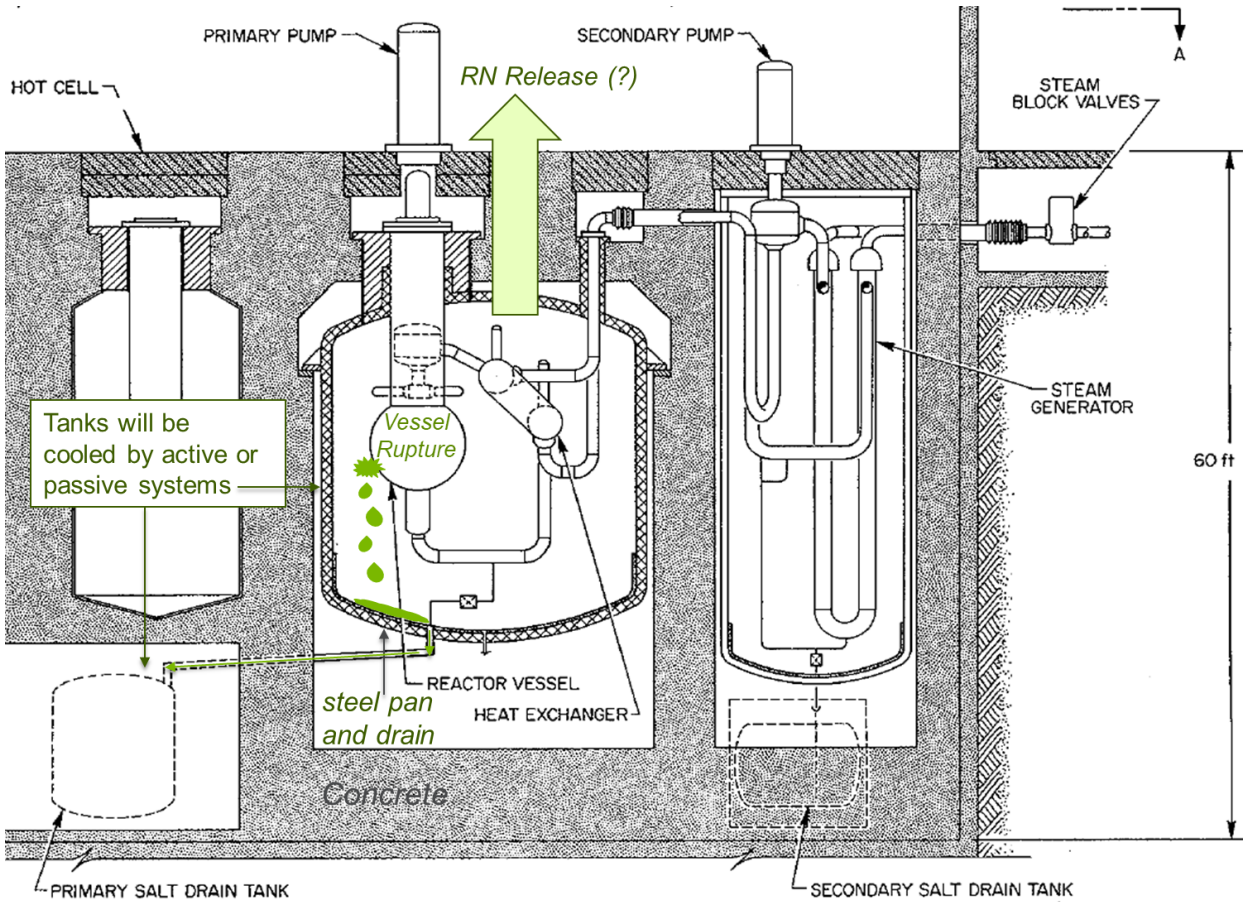


**Figure 19.** Schematic diagram of salt spill in primary containment cell due to a vessel rupture event (adapted from McWherter, J., Molten Salt Breeder Experiment Design Bases, ORNL-TM-3177, November 1970).

### *6.1.1 Description of Salt Spill Event*

Figure 19 shows a schematic layout of a salt spill accident within the primary loop containment cell of the molten salt breeder reactor experiment design. The steel guard pan and drain tank are protective measures that will likely be an element of any large MSR design to avoid the undesirable interaction of the spilled fuel salt with any concrete surfaces. The interaction of fuel salt and concrete results in concrete dehydration and gas generation, which could lead to containment pressurization. This will be avoided by covering all concrete structures that could receive a salt spill with steel or some other appropriate alloy. The steel guard pan will be angled such that the spilled salt will flow by gravity into a passively cooled drain tank.[1]

The effectiveness of designs to reject decay heat from the spilled salt is of primary concern due to uncertainties regarding the mechanisms of cooling and the undesirable implications of an uncontrolled rise in salt temperature. Such negative implications include:

- the vaporization and transport of fission products such as Cs and I and possibly actinides within containment (a possible radionuclide source term),
- the generation and transport of corrosive gaseous fluoride or chloride species that could cause accelerated corrosion of alloys within the core containment cell,
- the heating and possible degassing of concrete below the catch pan ($H_2O$ and $CO_2$ release).

In addition to thermal radiation and convection, decay heat will likely be rejected from the spilled fuel salt by cooling systems between the steel catch pan and concrete or within the concrete itself. The drain tank will also be cooled by either active or passive means. The amount of decay heat that will need to be rejected from the spilled fuel salt will depend on the power density of the salt. It is estimated that the fuel salt will continue to produce ~7% of full power immediately after fission stops. This implies that several tens of megawatts will need to be rejected for several days after salt is spilled from a large reactor (2500 MWth). The corresponding power densities for MSR fuel salts will range from 20 – 50 $MW/m^3$ at shutdown.

Accident progression for fuel salt loop rupture depends on the type and configuration of the passive decay heat removal system. Passive decay heat removal mechanisms are categorized based on their means of thermal coupling to the fuel salt. Direct Reactor Auxiliary Cooling Systems (DRACS) couple to the fuel salt by direct contact with the fuel salt, reactor vessel, or drain tank (by heat exchangers inside the reactor vessel or part of the reactor vessel) and employ natural circulation to transfer the heat to an environmentally-coupled heat exchanger. A Reactor Vessel Auxiliary Cooling System (RVACS) relies on radiative heat transfer from the reactor vessel, spilled fuel salt, or drain tank and convective heat transfer by the containment atmosphere to a natural convection driven heat transfer loop. A Pool Reactor Auxiliary Cooling System (PRACS) immerses the fuel salt loop in a tank or pool of liquid coolant (typically another salt) to provide shielding and additional thermal mass (coping time). PRACS systems eventually transfer decay heat to another natural circulation driven heat removal system (DRACS or RVACS). Regardless of the type of heat removal system employed for a given MSR, questions remain regarding the processes involved in decay heat rejection from a spilled mass of salt. By quantifying these processes, the planned experiments may inform design decisions regarding which decay heat removal system is most efficient and safe for a given fuel salt composition and primary loop design.

[1] It is important to note that salt could contact concrete if the steel catch pan fails. In reviewing the PRISM (sodium-cooled fast reactor), the NRC questioned what would happen if a steel liner in a room containing a sodium spill failed, resulting in sodium contact and interaction with underlying concrete. Several large-scale tests were conducted at Sandia to look at sodium interaction with concrete and a code was developed to assess this type of interaction. When concrete decomposes, it gives off water and $CO_2$, both of which may affect the salt chemistry and could cause a pressure stress on containment seals.

### *6.1.2 Engineering Scale Tests: Salt Spill Morphology and Spreading*

Argonne has extensive experimental experience with melt spreading behavior for ex-vessel LWR accident scenarios (e.g., Farmer, 2017) as well as convective cooling of melts within crucible-type geometries (e.g., Farmer, 2018). These studies have been used to parametrize and validate MELCOR models for LWR accident scenarios and have led to generalized observations that are applicable to the MSR fuel salt spill scenarios being considered. One such observation is that the salt spill "pour" rate and salt temperature have a large impact on the morphology and eventual location of the post-spread fuel salt accumulation. These are two parameters that must be quantified using engineering-scale tests.

Key issues that the engineering scale tests can address are:

- What is the extent of spreading of the liquid salt once the reactor vessel or primary circuit pipe is breached as a function of the salt pour rate and temperature? It is possible that a mound of salt will form on the catch pan at low temperatures and flowrates.[2] For a pour of this type, will the material that flows down the vent line to the dump tank freeze inside the pipe and plug it?

- Once the material is inside the drain tank, a situation will develop in which the melt pool, heated by decay of fission products inside the salt, dissipates heat to the tank walls and cooling system. The equilibrium temperature reached by the salt once in the tank will be determined by the natural convection heat transfer coefficients to the tank sidewalls, bottom surface, and top surface. Heat transfer up will also need to factor in the convective/radiative heat transfer from the melt upper surface to the upper tank structures. It is important to know (1) values of these heat transfer coefficients (usually modeled and then confirmed through experiments) and (2) the time-dependent decay heat level in the salt volume that will establish the salt pool equilibrium temperature and the rate at which the decay heat can be dissipated to the surrounding environment/heat rejection system. The equilibrium salt temperature also affects fission product release from the molten salt pool.

- Structural questions regarding the consequences of the possible warping of steel liners and catch pans exposed to high temperature salts are also important. Extensive warping could lead to a failure of the designed function of the catch pan or liner and salt drainage.

- Findings from Fukushima indicate that melt released from the reactor vessel can extensively freeze on and below the vessel structure and not be cooled by water injected to the containment floor to cool the melt. Decay heat from material frozen on structures is dumped directly to the containment atmosphere and could stress containment seals. Applying these insights to a salt-cooled reactor, solidified salt on the catch pan will remain in place for decades until the plant is eventually taken down and the salt recovered. This raises concerns about long-term corrosion of the liner and whether it could eventually fail. Fukushima illustrated that long-term containment response and integrity following an accident had not been fully thought through. Long-term containment is now being considered by the NRC and others.

- Another concern is that salt frozen on the liner will continue to dissipate heat both upwards into containment and downwards to the underlying concrete. Typically, insulation would be placed between a catch pan and the concrete to minimize heating of the concrete during a spill as heat up of the concrete can release $H_2O$ and $CO_2$ without direct contact by hot salt. This gas production can place additional loads (by pressurization) on the catch pan. Even when insulated, there is a

[2] For example, a large and deep (2-3 meters) accumulation of core debris has been found beneath the reactor vessel at Unit 3 at Fukushima Daiichi.

possibility for the underlying concrete to eventually heat up since concrete is an extremely poor heat sink (thermal conductivity < 1 W/m-K).

A proposed study of fuel salt property measurements and salt spill tests is included as Appendix A. Results of that study can be used to develop and validate the MST for a salt spill bounding accident.

# 7 Conclusions and Recommendations for Future Work

This report provides an in-depth critical review of the information that is needed to inform MST models for liquid fueled MSRs. NRC staff stated in SECY-93-092 that an MST should be developed from phenomenological models of radionuclide transport from the fuel to the environment and consider holdup volumes, barriers to release, and phenomena that inhibit or slow transport. One of the first steps towards achieving MST modeling capability involves identifying and characterizing radionuclide sources and ranking radionuclides in order of dose consequence. The important radionuclides for a generic MSR from a radiotoxicity perspective include Cs, I, Sr, Ru, Ce, and any of the actinides. Sources of radionuclides include the fuel salt, coolant salt (due to activation of coolant components), cover gas, off gas system, and fuel processing system.

MST modeling of MSRs also requires an understanding of possible radionuclide partitioning phenomena both during normal operation and during identified accident scenarios. In general, the volatile radionuclides are most likely to be released during normal operation or an accident. The volatile fission product species include noble gases (Xe and Kr), volatile halogen species (HF, $F_2$, $Cl_2$, $Br_2$, $I_2$, CsI), and volatile tritium species ($^3H_{2(g)}$, $^3HH_{(g)}$, and $^3HF_{(g)}$). Under most conditions, the actinides will be retained as dissolved fluoride and chloride complexes in fluoride and chloride fuel salts, respectively. It is important to note that $F_2$ or $Cl_2$ radiolysis products can lead to the formation of volatile $UF_6$ in fluoride salts and relatively volatile $UCl_4$ in chloride salts. The precipitation or plate out of metals can disrupt fuel salt flow and generate decay heat in concentrated areas. In addition, the precipitation of fissile material in the fuel salt could violate the reactivity control fundamental safety function (FSF). This could occur by the formation of metallic actinides under reducing conditions or from disproportionation reactions, the formation of insoluble actinide oxides due to reaction with $H_2O$ or $O_2$, formation of uranium carbides due to reaction with the graphite moderator, or decreased actinide solubility due to the buildup of fission products in the fuel salt. Physical transport phenomena must also be considered including the transport of non-volatile radionuclides into the cover gas region entrained in noble gas bubbles or as sprayed mists.

Accurately modeling the chemical and physical phenomena described above will require a rigorous experimental program to provide fundamental thermochemical and thermophysical data and model validation. Remaining thermophysical and thermochemical data gaps have been identified by Jerden et al. (2019b) and McMurray et al. (2019).

MSTs also require the identification of accident scenarios to quantify potential radionuclide release. The proposed methodology for choosing an accident to evaluate MSR safety in the near-term is based on a conservative bounding approach rather than the type of probabilistic or deterministic analyses used for LWR source term studies. The bounding approach is being employed because of the relative immaturity of MSR technologies and the fact that it enables the development of consequence information to support severe accident evaluation without requiring a time-consuming probabilistic risk assessment that would likely be complicated by a lack of data and design uncertainties. This proposed safety evaluation method is tailored for MSRs and relies upon a combination of bounding accident analysis, defense-in-depth provided through functional containment, and process hazard assessment to demonstrate fulfillment of fundamental safety functions (viz. preventing radionuclide release to the environment, controlling nuclear reactivity and providing sufficient decay heat rejection during transient and accident events). The bounding accidents of

interest include ruptures in fuel salt loop, primary heat exchanger tubing, cover gas/off gas system, or fuel processing system. The maximum credible accident for MSRs likely involves the rupture of the fuel salt loop, leading to hot fuel salt spilling onto the containment floor (see Section 6.1 for details).

The salt spill simulation for a LiF-$ThF_4$-$UF_4$-Cs-I system by Kalilainen et al. (2020) is one of the first MST trial calculations for an MSR bounding accident and provides valuable preliminary results to consider for future MSR MST models:

- The amount and timing of release of key radionuclides from the spilled fuel salt differed significantly when excess Gibbs energy of mixing was considered compared to when only the vapor pressures of pure species were included in thermochemical models. Specifically, the retention of all key species modeled (CsI, CsF, LiI, $ThF_4$, $UF_4$, $UF_3$) increased dramatically when non-ideal mixing was considered.

- Depressurization in containment increased the amount of evaporated materials by altering the mass transfer coefficient at the salt surface.

- The total amount of fluorine in the salt greatly affected iodine speciation. Excess fluorine (2% greater than the fuel salt stoichiometric value) prevented the formation of CsI and led to the formation of highly volatile $I_2$.

- Many of the species included in the model evaporated at normal operating temperatures of MSRs (900 K – 1000 K).

Kalilainen et al. (2020) offer guidance to improve future MST models for fission product and actinide release from an evaporating fuel salt spill. Future studies will need to account for all of the fission products discussed in Section 3.2 in addition to Cs and I, which will improve accuracy. The effect of over and under fluorination should be more thoroughly modeled due to the demonstrated effect of total fluorine on fission product speciation and the known effect of salt redox potential on containment structure corrosion. Future modeling efforts will also need to represent a more complex containment structure and include more details on passive decay heat removal systems and the fuel drain tanks.

Another limitation with the approach of Kalilainen et al. (2020) is the lack of available information on the thermo-physical and thermo-hydraulic behavior of the salt. For example, the spilled salt is modelled to be a flat, homogeneous mass of liquid, while in actuality there may be inhomogeneities and solid polycrystalline crusts that form on the top and bottom of the spilled salt mass. These and other data gap issues require focused experimental investigations that are discussed in Section 6.1 and Appendix A.

## References

ASME/ANS, "Probabilistic Risk Assessment Standard for Advanced Non-LWR Nuclear Power Plants," RA-S-1.4-2013, 2013.

Barton, C. J., "Solubility of Plutonium Trifluoride in Fused-Alkali Fluoride—Beryllium Fluoride Mixtures," *The Journal of Physical Chemistry*, vol. 64, issue 3, pp. 306-309, 1960.

Beall, S. E., Haubenreich, P. N., Lindauer, R. B., and Tallackson, J. R., "MSRE Design and Operation Report, Part V, Reactor Safety Analysis Report," ORNL-TM-732, p. 240, 1964.

Bell, M. J., "Calculated Radioactivity of the MSRE Fuel Salt," ORNL/TM-2970, 1970.

Bettis, E. S. and Robertson, R. C., "The Design and Performance Features of a Single-Fluid Molten Salt Breeder Reactor," *Nuclear Applied Technology*, vol. 8, issue 2, pp. 190–207, 1970.

Bettis, E., Alexander, L., Watts, H., "Design Studies of a Molten-Salt Reactor Demonstration Plant," ORNL-TM-3832, 1972

Burris, L., Dillon, I., "Estimation of Fission Product Spectra in Discharged Fuel from Fast Reactors," ANL-5742, 1957

Capelli, E., Beneš, O. and Konings, R. J. M., "Thermodynamics of Soluble Fission Products Cesium and Iodine in the Molten Salt Reactor," *Journal of Nuclear Materials*, vol. 501, pp. 238-252, 2018.

Code of Federal Regulations: 10 § 100, "Reactor Site Criteria," Amended 2013.

Code of Federal Regulations: 10 § 50.67, "Accident Source Term," Amended 1999.

Compere, E., Kirslis, S., Bohlmann, E., Blankenship, F., Grimes, W., "Fission Product Behavior in the Molten Salt Reactor Experiment," ORNL-4865, 1975.

Delpech, S., Merle-Lucotte, E., Heuer, D. et al., "Reactor Physic and Reprocessing Scheme for Innovative Molten Salt Reactor System," *Journal of Fluorine Chemistry*, vol. 130, issue 1, pp. 11–17, 2009.

DiNunno, J., Baker, R. E., Anderson, F. D., and Waterfield, R. L., "Calculation of Distance Factors for Power and Test Reactor Sites," TID-14844, 1962.

Eckerman, K., Wolbarst, A., Richardson A., "Limiting Values of Radionuclide Intake and Air Concentration and Dose Conversion Factors for Inhalation, Submersion, and Ingestion," EPA-520/1-88-020, 1988.

Engel, J., Bauman, H., Dearing, J., Grimes, W., McCoy, H., "Development Status and Potential Program for Development of Proliferation-Resistant Molten-Salt Reactors," ORNL/TM-6415, 1979.

Ergen, W. K., Callihan, A. D., Mills, C. B., and Dunlap Scott, "The Aircraft Reactor Experiment—Physics," *Nuclear Science and Engineering*, vol. 2, pp. 826-840, 1957.

Farmer, M., "The CORQUENCH Code for Modeling of Ex-Vessel Corium Coolability under Top Flooding Conditions Code Manual – Version4.1-beta," ANL-18/22, 2018.

Farmer, M., "The MELTSPREAD Code for Modeling of Ex-Vessel Core Debris Spreading Behavior, Code Manual – Version3-beta," ANL/NE-17/20, 2017.

Flanagan, G. F., Holcomb, D. E., and Poore III, W. P., "Molten Salt Reactor Fuel Qualification Considerations and Challenges," ORNL/LTR-2018/1045, 2018.

GEMS, "GEM Software (GEMS) Home," Paul Scherrer Institut. [Online] http://gems.web.psi.ch.

Gérardin, D., Uggenti, C. A., Beils, S., Carpignano, A., Dulla, S., Merle, E., Heuer, D., Laureau, A., Allibert, M., "A Methodology for the Identification of the Postulated Initiating Events of the Molten Salt Fast Reactor", *Nuclear Engineering and Technology*, vol. 51, pp. 1024 -1031, 2019.

Grabaskas, D., Brunett, A. J., M. Bucknor, M., J. Sienicki, J., Sofu, T., 2015, "Regulatory Technology Development Plan - Sodium Fast Reactor: Mechanistic Source Term Development," ANL-ART-3, 2015.

Grabaskas, D., Bucknor, M., Jerden, J., Brunett, A. J., Denman, M., Clark, A., Denning, R. S., "Regulatory Technology Development Plan-Sodium Fast Reactor: Mechanistic Source Term–Trial Calculation", ANL-ART-49, Argonne National Laboratory, 2016a.

Grabaskas, D., Bucknor, M., Jerden, J., "Regulatory Technology Development Plan - Sodium Fast Reactor: Mechanistic Source Term Development - Metal Fuel Radionuclide Release," ANL-ART-38, 2016b.

Grimes, W. R., "Molten Salt Reactor Chemistry," *Nuclear Applied Technology*, vol. 8, issue 2, pp. 137–155, 1970.

Grimes, W. R., "Molten-Salt Reactor Program Semiannual Progress Report," ORNL-3708, pp. 238, 1964.

Haubenreich, P. N. and Engel, J. R., "Experience with the Molten-Salt Reactor Experiment," *Nuclear Applied Technology*, vol. 8, issue 2, pp. 118–136, 1970.

Hombourger, B., Krepel, J., Pautz, A., The EQL0D Procedure for Fuel Cycle Studies in Molten Salt Reactors and its Application to the Transition to Equilibrium of Selected Designs," *Annals of Nuclear Energy*, vol. 144, pp. 107504, 2020.

Icenhour, A. S., Williams, D. F., Trowbridge, L. D., Toth, L. M., and Del Cul, G. D., "An Overview of Radiolysis Studies for the Molten Salt Reactor Remediation Project," *Proceedings of Global 2001*, Paris, France, 2001.

Idaho National Laboratory, "Mechanistic Source Term White Paper," INL/EXT-10-17997, 2010.

Ignatiev, V., Feynberg, O. et al., "Progress in Development of Li, Be, Na/F Molten Salt Actinide Recycler and Transmuter Concept," *In Proceedings of ICAPP*, Nice, France. pp. 3004–3013, 2007.

Jerden, J., Grabaskas, D., Bucknor, M., "Development of a Mechanistic Source Term Approach for Liquid-Fueled Molten Salt Reactors," ANL/CFCT-19/4, Argonne National Laboratory, 2019a.

Jerden, J. "Molten Salt Thermophysical Properties Database Development: 2019 Update," ANL/CFCT-19/6, 2019b.

Kalilainen, J., Nichenko, S., and Krepel, J., "Evaporation of Materials from the Molten Salt Reactor Fuel under Elevated Temperatures," *Journal of Nuclear Materials*. pp. 152134, 2020.

Kloosterman, J., "Safety Assessment of the Molten Salt Fast Reactor (SAMOFAR)," in Molten Salt Reactors and Thorium Energy (Editor: T. J. Dolan), pp. 565-569, Woodhead Publishing, June 2017.

Lizin, A., Tomilin, S., Ponomarev, L., Fedorov, Y., Hirose, Y., "Fast-Spectrum, Liquid-Fueled Reactors," in Molten Salt Reactors and Thorium Energy (Editor: T. J. Dolan), Woodhead Publishing, pp. 375-433, 2017.

Mathieu, L., Heuer, D., Merle-Lucotte, E. et al., "Possible Configurations for the Thorium Molten Salt Reactor and Advantages of the Fast Non Moderated Version," *Nuclear Science and Engineering*, vol. 161, issue 1, pp. 78–89, 2009.

McFarlane, J., Ezell, N., Del Cul, G., Holcomb, D.E., Myhre, K., Chapel, A., Lines, A., Bryan, S., Felmy, H.M. and Riley, B., "Fission Product Volatility and Off-Gas Systems for Molten Salt Reactors," ORNL/TM-2019/1266, 2019.

McMurray, J. W., Besmann, T. M., Ard, J., FItzpatrick, B., Piro, M., Jerden, J., Williamson, M., Collins, B. S., Betzler, B. R. and Qualls, A. L., "Multi-Physics Simulations for Molten Salt Reactor Evaluation: Chemistry Modeling and Database Development," ORNL/SPR-2018/864. 2018.

McMurray, J., Besmann, T., Ard, J., Utlak, S., and Lefebvre, R., "Status of the Molten Salt Thermodynamic Database, MSTDB," ORNL/SPR-2019/1208. 2019.

McWherter, J. R., "Molten Salt Breeder Experiment Design Bases," ORNL-TM-3177, 1970.

Merle-Lucotte, E., Allibert, M., Brovchenko, M., Ghetta, V., Heuer, D., and Rubiolo, P., "Preliminary Design Assessment of the Molten Salt Fast Reactor," *In Actes de la conférence European Nuclear Conference ENC2012*, Manchester, UK, 2012.

Mourogov, A. and Bokov, P., "Potentialities of the Fast Spectrum Molten Salt Reactor Concept: REBUS-3700," *Energy Conversion and Management*, vol. 47, pp. 2761–2771, 2006.

NRC, "Assumptions Used for Evaluating the Potential Radiological Consequences of a Loss of Coolant Accident for Boiling Water Reactors," U.S. Nuclear Regulatory Commission Regulatory Guide 1.3 Revision 2, 1974a.

NRC, "Assumptions Used for Evaluating the Potential Radiological Consequences of a Loss of Coolant Accident for Pressurized Water Reactors," U.S. Nuclear Regulatory Commission Regulatory Guide 1.4 Revision 2, 1974b.

NRC, "Draft Preapplication Safety Evaluation Report for the Modular High-Temperature Gas-Cooled Reactor," U.S. Nuclear Regulatory Commission Report NUREG-1338, 1989.

NRC, "Issues Pertaining to the Advanced Reactor (PRISM, MHTGR, and PIUS) and CANDU 3 Designs and their Relationship to Current Regulatory Requirements," U.S. Nuclear Regulatory Commission SECY-93-092, 1993.

NRC, "Accident Source Terms for Light-Water Nuclear Power Plants," U.S. Nuclear Regulatory Commission Report NUREG-1465, 1995.

NRC, "Alternative Radiological Source Terms for Evaluating Design Basis Accidents at Nuclear Power Reactors," U.S. Nuclear Regulatory Commission Regulatory Guide 1.183, 2000.

NRC, "Policy Issues Related to Licensing Non-Light Water Reactor Designs," U.S. Nuclear Regulatory Commission report SECY-03-0047, 2003.

NRC, "Second Status Paper on the Staff's Proposed Regulatory Structure for New Plant Licensing and Update on Policy Issues Related to New Plant Licensing," U.S. Nuclear Regulatory Commission report SECY-05-0006, 2005.

NRC, "Assessment of White Paper Submittals on Fuel Qualification and Mechanistic Source Terms (Revision 1) - Next Generation Nuclear Plant," ML14174A845, 2014.

NRC, "Accident Source Terms and Siting for Small Modular Reactors and Non-Light Water Reactors," U.S. Nuclear Regulatory Commission report SECY-16-0012, 2016.

Phillips, J.E. and Easterly, C.E., "Sources of Tritium," ORNL/TM-6402, 1980.

Robertson, R., "Conceptual Design Study of a Single-Fluid Molten-Salt Breeder Reactor," ORNL-4551, 1971.

Rosenthal, M., Haubenreich, P., Briggs, R., "The Development Status of Molten-Salt Breeder Reactors," ORNL-4812, 1972.

Sekiguchi, Y., Uozumi, K., Koyama, T., and Terai, T., "Fundamental Study on the Vaporization of Cesium and Iodine Dissolved in LiF-NaF-KF Molten Salt," *Journal of Nuclear Materials*, vol. 522, pp. 136-143. 2019.

Shahbazi, S. and Grabaskas, D., "Functional Requirements for the Modeling and Simulation of Advanced (Non-LWR) Reactor Mechanistic Source Term," ANL/NSE-20/17, 2020.

Shcherbina, N., Kivel, N., Günther-Leopold, I., Kulik, D., Bertsch, J., HERACLES Project and Thermodynamic Database Homepage. [Online] http://www.psi.ch/heracles/

Slessarev, I. and Bokov, P., "On Potential of Thermo-Nuclear Fusion as a Candidate for External Neutron Source in Hybrid Systems (Applied to the "WISE" Concept)," *Annals of Nuclear Energy*, vol. 30, issue 16, pp. 1691–1698, 2003.

Steunenberg, R., Pierce, R., Burris, L., "Pyrometallurgical and Pyrochemical Fuel Processing Methods," Progress in Nuclear Energy Series III, Process Chemistry, vol. 4(New York: Pergamon Press), pp. 461–504, 1969.

Taira, M., Arita, Y. and Yamawaki, M., "The Evaporation Behavior of Volatile Fission Products in FLiNaK Salt," *The Open Access Journal of Science and Technology*, vol. 5, issue 5, pp. 1-17, 2017.

Taube, M. and Ligou, J., "Molten Chlorides Fast Breeder Reactor Problems and Possibilities," *EIR-Bericht Nr. 215*, 1972.

Taube, M., "Fast Reactors Using Molten Chloride Salts as Fuel," *EIR-Bericht Nr. 332*, 1978.

Toth, L. M., Del Cul, G. D., Dai, S. and Metcalf, D. H., "Molten Fluoride Fuel Salt Chemistry," *In AIP conference proceedings,* vol. 346, issue 1, pp. 617-626, 1995.

Wang, S., Massone, M., Rineiski, A., Merle-Lucotte, E., Laureau, A., Gérardin, D., Heuer, D., Allibert, M., "A Passive Decay Heat Removal System for Emergency Draining Tanks of Molten Salt Reactors," *Nuclear Engineering and Design*, vol. 341, pp. 423-431, 2019.

Whatley, M. E., McNeese, L. E., Carter, W. L., Ferris, L. M., and Nicholson, E. L., "Engineering Development of the MSBR Fuel Recycle," *Nuclear Applied Technology*, vol. 8, issue 2, pp. 170–178, 1970.

Williams, D. F., Del Cul, G. D., and Toth, L. M., "A Descriptive Model of the Molten Salt Reactor Experiment After Shutdown: Review of FY 1995 Progress," ORNL/TM-13142. 1996.

Wright, A. L., "Primary System Fission Product Release and Transport," ORNL/TM-12681, 1994.

Yoshioka, R. and Kinoshita, M., "Liquid Fuel, Thermal Neutron Spectrum Reactors." In *Molten salt reactors and thorium energy*, pp. 281-373. Woodhead Publishing, 2017.

Yoshioka, R., Shimazu, Y., Mitachi, K., "Guidelines for MSR Accident Analysis," *Thorium Energy Conference (ThEC12)*, Shanghai, October 2012.

Zhang, J., "Electrochemistry of Actinides and Fission Products in Molten Salts—Data review," *Journal of Nuclear Materials*, vol. 447, pp. 271–284, 2014.

Zhang, J., Forsberg, C. W., Simpson, M. F., Guo, S., Lam, S. T., Scarlat, R. O., Carotti, F., Chan, K. J., Singh, P. M., Doniger, W. and Sridharan, K., "Redox Potential Control in Molten Salt Systems for Corrosion Mitigation," *Corrosion Science*, vol. 144, pp. 44-53, 2018.

# Appendix A: Conceptual Plan to Validate Bounding Accident Models

A two-part study including fuel salt property measurements and salt spill tests is proposed to generate a generic set of data and observations that can be used to parameterize and validate models quantifying radionuclide source terms and thermo-hydraulic conditions during a generic MSR salt spill accident. The test conditions used in the study are not intended to represent a particular reactor design or concept. Rather, generic conditions are used to inform various commercial designs being considered.

Conceptual test plans are provided for the two parts of the study. The first part includes small-scale laboratory measurements to quantify the thermo-physical property values of fuel salts that are needed to parameterize new thermo-hydraulic and radionuclide release models over an accident-relevant temperature range. Those results will guide the design of engineering scale thermal-hydraulic tests representing salt spill accident scenarios performed in the second part of the study. The property measurements and thermal-hydraulic tests will be performed using uranium-bearing fluoride and chloride simulated fuel salts made by doping base salts FLiNaK and NaCl-$UCl_3$ with relevant concentrations of surrogate fission products. Using these base salt systems will leverage results and insights from on-going activities in the DOE Molten Salt Reactor Campaign. The most important fission products from a dose consequence perspective are radioisotopes of Cs, I, Sr, Ru, and Ce (see Section 3.2 and Figure 5). Salt mixtures will be made with different concentrations of nonradioactive isotopes of these elements for use in property measurements and corrosion tests. Larger amounts of selected compositions will be prepared for use in the engineering-scale spill tests.

**Part 1: Thermo-physical Property Measurements**

Development of a physico-chemical model for a salt spill accident progression will require quantification of the thermo-hydraulic properties of the spilled fuel salt based on thermophysical and thermochemical property values of fuel salts of interest. The temperature range over which these properties need to be known will depend on the type and composition of the fuel salt, the reactor design, and the nature of the accident. Based on the discussion in Section **Error! Reference source not found.**, the maximum temperature of the spilled fuel salt is expected to be approximately 1300 $^{o}$C. Therefore, the temperature range relevant to salt spill scenarios is from the melting point to 1300 $^{o}$C. **Error! Reference source not found.** identifies salt properties that need to be measured over this range and lists methods currently being used in the Argonne Chemical and Fuel Cycle Technologies division and methods that can be readily implemented.

Part 1 of the study will include property measurements listed in Table A-1 for simulated chloride and fluoride fuel salts and laboratory corrosion tests to quantify and characterize the corrosion behaviors of optional catch pan materials in the different surrogate fuel salts. 316SS will be used in initial corrosion tests and alloys considered for use in reactor designs or in the test apparatuses to be used in Part 2 will be used in subsequent corrosion tests. Property measurements will be made for several salts with different dopant contents to assess the sensitivity of the property value to the fission product content. Electrochemical test methods developed to characterize material corrosion behavior and measure corrosion rates in molten salts under different redox conditions will be used to map out the corrosion behavior over a range of conditions. Corrosion measurements will span the temperature range of the salt spill accident scenario from just above the melting point to approximately 1300 $^{o}$C or the highest temperature that can be attained and a range of redox conditions. Post-test examinations will include metallurgical analysis of the steel/salt interface to further characterize the extent of interaction, including optical and scanning electron microscopy of corroded surfaces and polished cross sections.

**Table A-1**. Required salt property values and existing capabilities in CFCT

| **Property** | **Method** | **Status of Capability** |
|---|---|---|
| Density of liquid and solids *(including localized salt crust)* | Archimedes Method and direct measurement | Currently used for U-bearing salts. |
| Thermal conductivity of liquid and possible solids *(including localized salt crust)* | Laser Flash Analysis System | |
| Liquid Viscosity | Rotating Spindle Viscometer | |
| Heat capacities of liquid and solids *(including localized salt crust)* | Differential Scanning Calorimeter | |
| Salt boiling temperature | | |
| Latent heat of fusion of solid fuel salt | | |
| Liquidous/Solidus temperatures, including the impact of salt impurities | | |
| Volume expansion coefficient of fuel salt and possible solid crusts | Calculated from density measurements | |
| Aerosol analyses of gas samples taken for vapor pressure measurements | Filter and microscopic characterization SEM-EDS | |
| Surface tension of molten fuel salt | Variation of Archimedes Method | Technique is established, experimental set up required |
| Radiation emissivity | Infrared Camera | |
| Fission product vapor pressures (Cs, I, Sr, Ru, Ce) | In-line mass spectrometry | Sampling technique requires development |
| Uranium vapor pressure | | |

Results from the property measurements listed in **Error! Reference source not found.** and the corrosion tests can be used to parameterize a thermo-hydraulic model for the selected fuel salts at the relatively high accident temperatures. That model will form the basis for new accident progression and consequence models that can be incorporated into reactor accident progression codes such as MELCOR.

**Part 2: Engineering Scale Thermal-hydraulic Tests to Address Salt-Specific Accident Behavior**

Engineering scale spreading and tank retention thermal-hydraulic tests will be performed using doped salts that were characterized in the laboratory scale tests. Results and insights from the property measurements will be used to guide the design of engineering scale tests. The amount of salt to be used in each test will be based in part on a thermal-hydraulic scaling analysis aimed at representing values of key variables in the reactor. As much as 100 kg of each salt might be used in the thermal-hydraulic tests based on surface-to-volume considerations. The testing approaches, design, and how these tests might be conducted and equipment instrumented are summarized below. Separate test series will be performed with the selected fluoride and chloride salts.

**Salt Spreading Tests**

If the reactor vessel fails, salt will need to relocate across a catch pan and then flow through a vent line and into a tank. Molten salt from a melt generator will be dropped onto a steel plate leading to a vent line. The leading edge penetration, local salt temperatures, local plate temperature and stress response, and post-test spread distribution on the steel plate and in the vent line will be measured. The melt temperature and flowrate will be measured to determine extent of melt penetration. The releases of surrogate fission products from the molten salt will be measured during this phase. Aerosol sizes and concentrations in the vessel gas space will be measured by periodically drawing samples through cascade impactors. Chemical compositions of these aerosols will be determined by using SEM-EDS and ICP/OES to evaluate the fission product release fractions. Gas space chemical compositions will be measured by drawing a continuous sample through an on-line gas mass spectrometer at a fixed cover-gas flowrate to measure the release rates

of different isotopes. Post-test examinations will include metallurgical analysis of the steel/salt interface to further characterize the extent of interaction. Some property measurements may be made for samples of recovered salt. Data from these tests can be used to qualify salt spreading models that support plant design and licensing processes and to characterize fission product release into containment areas during this phase.

**Tank retention and long-term cooling Tests**

Once the salt is inside the vent tank, the melt pool will continue to be heated by the decay of fission products in the salt and dissipate heat to the tank walls and cooling system. The equilibrium temperature is affected by the natural convection heat transfer coefficients to the tank sidewalls, bottom surface, and top surface. Heat transfer assessments will need to factor in the convective-radiative heat transfer from the melt upper surface to the upper tank structures. It is important to determine the heat transfer coefficients because these will determine the equilibrium temperature at which the decay heat can be dissipated to the surrounding environment. It is important to know the equilibrium salt temperature because it affects fission product release from the pool. These tests will provide representative interaction values for the simulated chloride and fluoride fuel salts.

Molten salt from a melt generator will be poured into a simulated retention tank. The tank will be equipped with either Calrod® heaters or electrodes for direct electrical heating of the salt to simulate decay heat. Melt temperature and heat flux at the retention tank boundary are important to represent accurately because both impact the tank corrosion rate. The tank will be instrumented to measure salt temperatures at various axial and radial locations. The interior surface temperatures of the tank walls will be measured at several locations and the heat flux from the wall to the heat rejection system will be determined. This will allow convective heat transfer coefficients in the pool to be determined. The input power will be varied to simulate decay heat transfer and fission product release information will be acquired at several salt pool temperatures. The tank will also be equipped with a salt draw sample system and a gas phase sampling and analysis system. Some property measurements may be made for samples of recovered salt.

Results from the engineering-scale and laboratory tests will be compiled and compared for consistency. Property data for salt mixtures with different dopant levels will be provided for inclusion in the data base being assembled within the DOE MSR campaign. All test results will be documented in Laboratory reports.

**Chemical and Fuel Cycle Technologies Division**
Argonne National Laboratory
9700 South Cass Avenue, Bldg. 205
Argonne, IL 60439

www.anl.gov